INSTRUCTIONS ON THE ANNOTATION OF PDF FILES

To view, print and annotate your article you will need Adobe Reader version 9 (or higher). This program is freely available for a whole series of platforms that include PC, Mac, and UNIX and can be downloaded from http://get.adobe.com/reader/. The exact system requirements are given at the Adobe site: http://www.adobe.com/products/reader/tech-specs.html.

Note: if you opt to annotate the file with software other than Adobe Reader then please also highlight the appropriate place in the PDF file.

PDF ANNOTATIONS

Adobe Reader version 9

When you open the PDF file using Adobe Reader, the Commenting tool bar should be displayed automatically; if not, click on 'Tools', select 'Comment & Markup', then click on 'Show Comment & Markup tool bar' (or 'Show Commenting bar' on the Mac). If these options are not available in your Adobe Reader menus then it is possible that your Adobe Acrobat version is lower than 9 or the PDF has not been prepared properly.

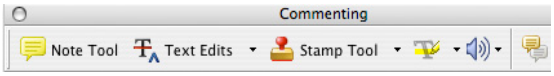

(Mac)

PDF ANNOTATIONS (Adobe Reader version 9)

The default for the Commenting tool bar is set to 'off' in version 9. To change this setting select 'Edit | Preferences', then 'Documents' (at left under 'Categories'), then select the option 'Never' for 'PDF/A View Mode'.

(Changing the default setting, Adobe version 9)

Adobe Reader version X

To make annotations in the PDF file, open the PDF file using Adobe Reader X, click on 'Comment'.

If this option is not available in your Adobe Reader menus then it is possible that your Adobe Acrobat version is lower than X or the PDF has not been prepared properly.

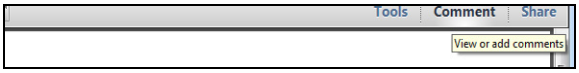

This opens a task pane and, below that, a list of all Comments in the text. These comments initially show all the changes made by our copyeditor to your file.

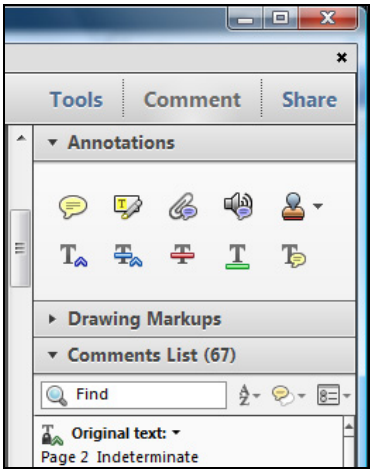

HOW TO...		
Action	**Adobe Reader version 9**	**Adobe Reader version X**
Insert text	Click the 'Text Edits' button on the Commenting tool bar. Click to set the cursor location in the text and simply start typing. The text will appear in a commenting box. You may also cut-and-paste text from another file into the commenting box. Close the box by clicking on 'x' in the top right-hand corner.	Click the 'Insert Text' icon on the Comment tool bar. Click to set the cursor location in the text and simply start typing. The text will appear in a commenting box. You may also cut-and-paste text from another file into the commenting box. Close the box by clicking on '_' in the top right-hand corner.
Replace text	Click the 'Text Edits' button on the Commenting tool bar. To highlight the text to be replaced, click and drag the cursor over the text. Then simply type in the replacement text. The replacement text will appear in a commenting box. You may also cut-and-paste text from another file into this box. To replace formatted text (an equation for example) please Attach a file (see below).	Click the 'Replace (Ins)' icon on the Comment tool bar. To highlight the text to be replaced, click and drag the cursor over the text. Then simply type in the replacement text. The replacement text will appear in a commenting box. You may also cut-and-paste text from another file into this box. To replace formatted text (an equation for example) please Attach a file (see below).
Remove text	Click the 'Text Edits' button on the Commenting tool bar. Click and drag over the text to be deleted. Then press the delete button on your keyboard. The text to be deleted will then be struck through.	Click the 'Strikethrough (Del)' icon on the Comment tool bar. Click and drag over the text to be deleted. Then press the delete button on your keyboard. The text to be deleted will then be struck through.
Highlight text/ make a comment	Click on the 'Highlight' button on the Commenting tool bar. Click and drag over the text. To make a comment, double click on the highlighted text and simply start typing.	Click on the 'Highlight Text' icon on the Comment tool bar. Click and drag over the text. To make a comment, double click on the highlighted text and simply start typing.
Attach a file	Click on the 'Attach a File' button on the Commenting tool bar. Click on the figure, table or formatted text to be replaced. A window will automatically open allowing you to attach the file. To make a comment, go to 'General' in the 'Properties' window, and then 'Description'. A graphic will appear in the PDF file indicating the insertion of a file.	Click on the 'Attach File' icon on the Comment tool bar. Click on the figure, table or formatted text to be replaced. A window will automatically open allowing you to attach the file. A graphic will appear indicating the insertion of a file.
Leave a note/ comment	Click on the 'Note Tool' button on the Commenting tool bar. Click to set the location of the note on the document and simply start typing. Do not use this feature to make text edits.	Click on the 'Add Sticky Note' icon on the Comment tool bar. Click to set the location of the note on the document and simply start typing. Do not use this feature to make text edits.

HOW TO...		
Action	**Adobe Reader version 9**	**Adobe Reader version X**
Review	To review your changes, click on the 'Show' button on the Commenting tool bar. Choose 'Show Comments List'. Navigate by clicking on a correction in the list. Alternatively, double click on any mark-up to open the commenting box.	Your changes will appear automatically in a list below the Comment tool bar. Navigate by clicking on a correction in the list. Alternatively, double click on any mark-up to open the commenting box.
Undo/delete change	To undo any changes made, use the right click button on your mouse (for PCs, Ctrl-Click for the Mac). Alternatively click on 'Edit' in the main Adobe menu and then 'Undo'. You can also delete edits using the right click (Ctrl-click on the Mac) and selecting 'Delete'.	To undo any changes made, use the right click button on your mouse (for PCs, Ctrl-Click for the Mac). Alternatively click on 'Edit' in the main Adobe menu and then 'Undo'. You can also delete edits using the right click (Ctrl-click on the Mac) and selecting 'Delete'.

PLEASE DO NOT ATTEMPT TO EDIT THE ARTICLE TEXT ITSELF

SEND YOUR ANNOTATED PDF FILE BACK TO ELSEVIER

Save the annotations to your file and return through the web interface as instructed. Before returning, please ensure you have answered any questions raised on the Query Form and that you have inserted all corrections: later inclusion of any subsequent corrections cannot be guaranteed.

FURTHER POINTS

- Any (grey) halftones (photographs, micrographs, etc.) are best viewed on screen, for which they are optimized, and your local printer may not be able to output the greys correctly.
- If the PDF files contain colour images, and if you do have a local colour printer available, then it will be likely that you will not be able to correctly reproduce the colours on it, as local variations can occur.
- If you print the PDF file attached, and notice some 'non-standard' output, please check if the problem is also present on screen. If the correct printer driver for your printer is not installed on your PC, the printed output will be distorted.

Please cite this article in press as: Ugel et al., Immune Tolerance to Tumor Antigens Occurs in a Specialized Environment of the Spleen, Cell Reports (2012), http://dx.doi.org/10.1016/j.celrep.2012.08.006

Cell Reports
Article

Cell PRESS
Open ACCESS

Immune Tolerance to Tumor Antigens Occurs in a Specialized Environment of the Spleen

Stefano Ugel,[1,2,7,8] Elisa Peranzoni,[2,7] Giacomo Desantis,[1] Mariacristina Chioda,[2] Steffen Walter,[3] Toni Weinschenk,[3] Jordi C. Ochando,[4] Anna Cabrelle,[5] Susanna Mandruzzato,[1,2] and Vincenzo Bronte[6,*]
[1]Department of Surgery, Oncology and Gastroenterology, University of Padua, 35128 Padua, Italy
[2]Istituto Oncologico Veneto, Istituto Di Ricovero e Cura a Carattere Scientifico, 35128 Padua, Italy
[3]Immatics Biotechnologies GmbH, 72076 Tübingen, Germany
[4]Centro Nacional de Microbiología, Instituto de Salud Carlos III, 28220 Madrid, Spain
[5]Venetian Institute for Molecular Medicine, 35129 Padua, Italy
[6]Verona University Hospital and Department of Pathology, 37134 Verona, Italy
[7]These authors contributed equally to this work.
[8]Present address: Ovarian Cancer Research Center, University of Pennsylvania, Philadelphia, PA 19104, USA
*Correspondence: vincenzo.bronte@univr.it
http://dx.doi.org/10.1016/j.celrep.2012.08.006

SUMMARY

Peripheral tolerance to tumor antigens (Ags) is a major hurdle for antitumor immunity. Draining lymph nodes are considered the privileged sites for Ag presentation to T cells and for the onset of peripheral tolerance. Here, we show that the spleen is fundamentally important for tumor-induced tolerance. Splenectomy restores lymphocyte function and induces tumor regression when coupled with immunotherapy. Splenic CD11b^{+}Gr-1^{int}Ly6C^{hi} cells, mostly comprising proliferating CCR2^{+}-inflammatory monocytes with features of myeloid progenitors, expand in the marginal zone of the spleen. Here, they alter the normal tissue cytoarchitecture and closely associate with memory CD8^{+} T cells, cross-presenting tumor Ags and causing their tolerization. Because of its high proliferative potential, this myeloid cell subset is also susceptible to low-dose chemotherapy, which can be exploited as an adjuvant to passive immunotherapy. CCL2 serum levels in cancer patients are directly related to the accumulation of immature myeloid cells and are predictive for overall survival in patients who develop a multipeptide response to cancer vaccines.

INTRODUCTION

The interaction between the immune system and transformed cells can result in the elimination of developing tumors, establishment of a growth dormancy state, or selection of neoplastic clones with the ability to survive in immune-competent hosts (Schreiber et al., 2011). On the other hand, cells of both innate and adaptive immunity can promote initial steps of cancer progression by fueling chronic inflammation in the tumor microenvironment (Grivennikov et al., 2010). Most experimental tumor models, as well as clinically diagnosed tumors, are analyzed when malignant cells may have already escaped early immune surveillance by both cell-autonomous and cell-independent mechanisms. At this stage, the almost universal feature of successfully progressive cancers is the activation of abnormal myelopoiesis and the recruitment of immature CD11b^{+}Gr-1^{+} myeloid cells into different tissues (Gabrilovich et al., 2012). This process is governed by tumor-released soluble factors and is dependent upon upregulation of key transcription factors in myeloid cells, such as cEBPβ (Marigo et al., 2010; Sonda et al., 2011). Myelopoiesis during acute infections, stress, or trauma results in rapid terminal differentiation of myeloid cells. In contrast, cancer myelopoiesis is associated with defective cell differentiation, leading to the accumulation and persistence of immature CD11b^{+}Gr-1^{+} myeloid elements (Gabrilovich and Nagaraj, 2009; Gabrilovich et al., 2012; Sica and Bronte, 2007). These cells can also cause profound alterations of antitumor immune responses. In fact, tumors bring on a progressive tolerance toward tumor antigens (Ags) among peripheral CD8^{+} T cells, which is orchestrated by the expansion of CD11b^{+}Gr-1^{+} cells (Dolcetti et al., 2010b; Kusmartsev et al., 2005; Nagaraj et al., 2007). The current view points toward the lymph node as the primary site for tumor Ag presentation and tolerance induction (Nagaraj et al., 2007), but accumulation of immature myeloid cells is extremely limited in these secondary lymphoid organs compared with other organs, such as the spleen. Although it was neglected for many years, the spleen is the main lymphoid organ that undergoes myeloid cell expansion during tumor development, and was recently found to possess unique biological properties. The spleen accumulates monocyte and granulocyte precursors that directly replenish tumor-associated macrophages and neutrophils during lung cancer development (Cortez-Retamozo et al., 2012). Moreover, the cords of the splenic subcapsular red pulp contain a reservoir of a peculiar monocyte subset that is promptly released in the bloodstream following acute injury (Swirski et al., 2009).

Please cite this article in press as: Ugel et al., Immune Tolerance to Tumor Antigens Occurs in a Specialized Environment of the Spleen, Cell Reports (2012), http://dx.doi.org/10.1016/j.celrep.2012.08.006

Cell PRESS
Open ACCESS

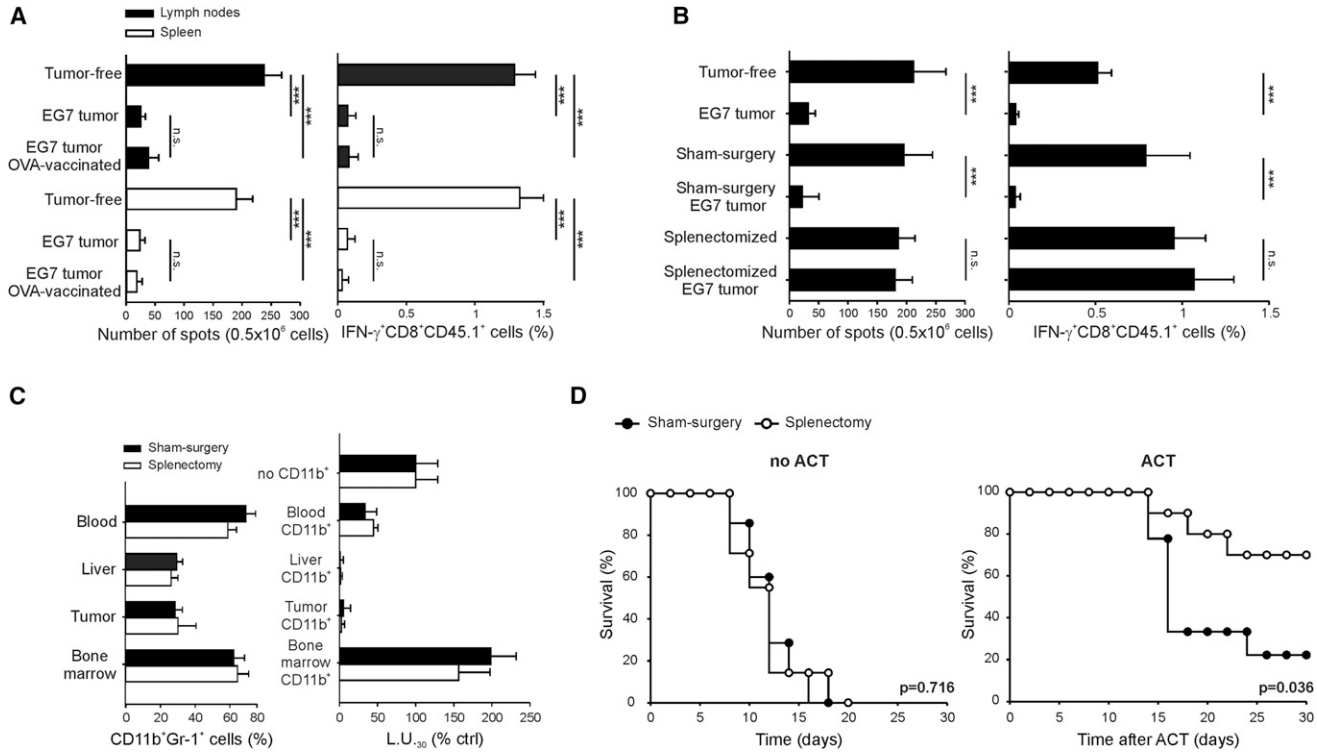

Figure 1. The Spleen Is a Key Organ for Tumor-Induced Tolerance

(A) C57BL/6 mice were either injected with 10^6 EG7 cells or not injected. After 7 days they received i.v. 5×10^6 naïve $CD8^+$ T cells isolated from the spleen of OT-1 mice. After 2 days the mice were vaccinated with $OVA_{257-264}$ peptide-pulsed DCs, and 5 days after vaccination, tumor-draining lymph nodes (black bar) and spleens (white bar) were removed, stimulated with either OVA peptide or unrelated peptide, and tested for IFN-γ production (ELISpot assay, left panel; intracellular staining, right panel). Data are presented as the difference in IFN-γ level (either as number of spots or percentage of cells) between OVA-peptide stimulation (specific stimulation) and β-gal peptide stimulation (unspecific stimulation). Data for intracellular stainings are presented as mean ± SD of the percentage of IFN-γ-producing $CD8^+CD45.1^+$ cells, from two independent experiments (n = 6 mice/group for each experiment). Statistical analysis was performed with Student's t test.

(B) C57BL/6 mice were splenectomized or subject to sham surgery. After 14 days, mice were either injected with 10^6 EG7 cells or not injected. Seven days after tumor challenge, the mice received i.v. 5×10^6 naïve $CD8^+$ T cells isolated from the spleen of OT-1 mice. After 7 days, the mice were sacrificed and tumor-draining lymph node cells were tested as in (A). Data are represented as mean ± SD of three experiments (n = 5 mice/group for each experiment). Statistical analysis was performed with Student's t test.

(C) When the tumor mass reached 1,000 mm^3, bone marrow, tumor, liver, and blood were collected and single-cell suspensions were analyzed for $CD11b^+Gr\text{-}1^+$ cell accumulation (left panel). $CD11b^+$ cells were immunomagnetically sorted from the same compartments and added in 1:2 serial dilutions (24% to 3% of the effector cells) to an MLPC to test their suppressive properties (right panel). The percentage of $L.U._{\text{-}30}$ of cultures containing 6% $CD11b^+$ cells is reported as the mean ± SD of two independent experiments. Data were normalized on the average value of $L.U._{\text{-}30}$ of MLPCs without $CD11b^+$ cells.

(D) Mice were either splenectomized or subjected to sham surgery. After 14 days, the mice were injected with 10^6 EG7 thymoma cells or not injected, and 7 days after tumor challenge the mice received i.v. 5×10^6 naïve $CD8^+$ T cells isolated from the spleen of OT-1 mice. A Kaplan-Meier survival analysis (n = 10 mice/group) was performed to compare splenectomy versus sham-surgery groups in the absence (left panel) and presence (right panel) of ACT.

See also Figure S1.

RESULTS

The Spleen Is Essential for Tumor-Induced Tolerance

We adoptively transferred naïve $CD8^+$ T cells from OT-1 mice bearing a T cell receptor specific for ovalbumin (OVA) and traced them in vivo using the congenic marker CD45.1. When we tested the ex vivo activation of peripheral OVA-specific $CD8^+$ T cells in mice bearing a tumor expressing the OVA model tumor Ag, we found that splenic lymphocytes, similarly to those taken from the lymph nodes, underwent Ag-specific tolerance (Figure 1A). Moreover, this state could not be reversed by in vivo immunization with the same tumor Ag delivered by dendritic cells (DCs) in a proper immune-stimulating context (Figure 1A). Therefore, we further investigated the role of the spleen in tumor-induced tolerance by performing the same type of tolerance assay in either splenectomized or sham-surgery-treated mice. Splenectomy completely restored lymphocyte activation by tumor Ag in tumor-draining lymph nodes (Figure 1B), and this effect could be readily observed even when OT-1 lymphocytes were stimulated in vitro with the OVA peptide before the adoptive transfer, or in vivo following vaccination with peptide-pulsed DCs (Figures S1A and S1B). The same results were obtained in mice from another strain, BALB/c, bearing 4T1 mammary carcinoma expressing influenza hemagglutinin (HA) model Ag (Figure S1C).

Cell PRESS
Open ACCESS

Of interest, splenectomy did not alter the distribution and suppressive function of CD11b$^+$Gr-1$^+$ myeloid cells in other tissues and blood, in at least three tumor models of different histology (Figure 1C; the results in EG7-bearing mice are shown here, but identical findings were obtained with MCA203 fibrosarcoma and LLC carcinoma, not shown). In contrast to a recent report (Cortez-Retamozo et al., 2012), splenectomy did not affect the rate of tumor growth in our models (Figure 1D, left panel); however, adoptive cell transfer (ACT) of tumor Ag-specific CD8$^+$ T cells in splenectomized mice led to a significant increase in survival compared with mice subjected to sham surgery (Figure 1D, right panel), further highlighting the importance of the splenic compartment in the systemic tolerization of CD8$^+$ T lymphocytes. These results strongly suggest that CD8$^+$ T cells in tumor-bearing mice go through a fundamental step for their inactivation in the spleen, and point to splenic CD11b$^+$Gr-1$^+$ cells as potential tolerogenic effectors.

Chemotherapy Increases the Efficacy of ACT by Eliminating Splenic CD11b$^+$Gr-1^{int} Cells

Chemotherapy can enhance the antitumor efficacy of ACT by several mechanisms, including the elimination of myeloid cells (reviewed in Gabrilovich et al., 2012; Ma et al., 2010; Restifo et al., 2012). To mimic experimentally the effect of splenectomy, we evaluated a large panel of conventional chemotherapeutic drugs for their ability to affect splenic CD11b$^+$Gr-1$^+$ cells and restore immune competence. We previously showed that the suppressive environment created by tumors does not allow the generation of Ag-specific cytotoxic T lymphocytes (CTLs) in alloantigen-stimulated cultures (mixed leukocyte culture [MLC]) set up with splenocytes of tumor-bearing mice (Bronte et al., 1998, 1999). In this initial screening, chemotherapy doses were selected as the lowest effective amount that did not affect tumor growth (Figure S2A). After low-dose chemotherapy, the functional rescue of allogeneic CTLs was achieved with some but not all of the tested drugs, and it was always paralleled by a significant decrease in the CD11b$^+$Gr-1^{int} cell population. In the same mice, CD11b$^+$Gr-1^{hi} and CD11b$^+$Gr-1^{lo} cell subsets were either poorly or not affected (Figures S2B and S2C). Moreover, all of the drugs that reestablished CTL function also rescued the percentages of CD3$^+$CD8$^+$ T cells in the spleen of tumor-bearing mice to the levels present in tumor-free mice, whereas the effects on CD3$^+$CD4$^+$ T cells were more drug dependent (Figure S2D).

Given the relationship between the depletion of the CD11b$^+$Gr-1^{int} cells subset and the recovery of CTL function, we evaluated whether the elimination of this cell subset could improve the efficacy of passive immunotherapy. To use a clinically relevant target, we employed a protocol based on the transfer of oligoclonal CTLs that recognize mouse telomerase (mTERT) Ag (Ugel et al., 2010), in combination with different chemotherapeutic agents. We employed two drugs that in our preliminary screening depleted splenic CD11b$^+$Gr-1^{int} cells and recovered CTL function (gemcitabine and 5-fluorouracil [5-FU]), and one drug that lacked these properties (docetaxel). The adoptive transfer of mTERT-specific CTLs in MCA203 fibrosarcoma-bearing mice had no effect on tumor regression unless it was preceded by treatment with either gemcitabine or 5-FU, but not with docetaxel (Figure 2A). All of these drugs, whether given alone or in combination with CTLs that recognize an irrelevant Ag, had no impact on either tumor growth or mouse survival. From the group of tested drugs, we selected 5-FU for further studies. For ~40 years, this pyrimidine analog has been adopted for the clinical treatment of various solid tumors, and particularly for breast cancer and gastrointestinal malignancies. Moreover, 5-FU does not cause immunogenic cancer-cell death of tumor cells (Vincent et al., 2010), which allowed us to focus on its effect on immune cells. To rule out the contribution of regulatory T lymphocytes and cytokine sinks operated by competing T lymphocytes and NK cells (Gattinoni et al., 2006) as a possible explanation for the immune benefits of 5-FU, we also tested the combinatorial therapy in immunodeficient *Rag2*$^{-/-}\gamma_c^{-/-}$ mice. A prolongation of mouse overall survival (OS) by a single inoculation of 5-FU before mTERT-specific ACT was observed in two different tumor models in *Rag2*$^{-/-}\gamma_c^{-/-}$ mice (Figure 2B). To maximize the adjuvant activity of chemotherapy, we exploited a schedule consisting of repeated administration of 5-FU in combination with mTERT-based ACT. In both immunocompetent and immunodeficient mouse strains, the growth of MCA203 tumor was controlled, resulting in prolonged survival for all of the treated mice (Figure 2C). No toxic side effects were recorded in the cohorts of mice during the duration of the treatment.

To verify that splenic CD11b$^+$Gr-1^{int} cells critically contributed to limit ACT efficacy, we isolated CD11b$^+$Gr-1^{hi} and CD11b$^+$Gr-1^{int} cells from the spleen of *Rag2*$^{-/-}\gamma_c^{-/-}$ tumor-bearing mice and transferred them into *Rag2*$^{-/-}\gamma_c^{-/-}$ tumor-bearing recipients that had received 5-FU 2 days earlier. The next day, the mice were adoptively transferred with mTERT-specific CTLs. Reconstitution with CD11b$^+$Gr-1^{int} cells, but not CD11b$^+$Gr-1^{hi} cells, abrogated the 5-FU immune adjuvant activity (Figure 2D), suggesting that this specific myeloid cell subset is critical for the impairment of antitumor immunity.

CD11b$^+$Gr-1^{int} Splenocytes Comprise Cycling, Committed Precursors that Resemble Inflammatory Monocytes

When we analyzed the kinetics of myeloid repopulation in the spleen of tumor-bearing mice following exposure to either control vehicle or 5-FU, we found that all of the myeloid subsets were initially affected by chemotherapy (Figure 3A), as expected. However, after administration of a single dose of 5-FU, CD11b$^+$Gr-1^{hi} and CD11b$^+$Gr-1^{lo} cells reached the numbers of untreated tumor-bearing mice in ~30 days, whereas this did not occur for CD11b$^+$Gr-1^{int} cells. The effect of 5-FU on CD11b$^+$Gr-1^{int} cells was indeed long-lasting, as in treated mice this cell subset was still ~15% of its counterpart in untreated control mice.

We also quantified the proliferative rate of different myeloid subsets in vivo by estimating the percentage of bromodeoxyuridine (BrdU)-incorporating cells after a 48 hr pulse with this synthetic nucleoside. While CD11b$^+$Gr-1^{hi} cells in the bone marrow were cycling, the same cell population was not proliferating in the spleen of tumor-free and tumor-bearing mice. On the contrary, CD11b$^+$Gr-1^{int} and CD11b$^+$Gr-1^{lo} cells were proliferating in the spleen and bone marrow of tumor-free mice, and when the tumor was present, the percentage of BrdU$^+$ cells

Please cite this article in press as: Ugel et al., Immune Tolerance to Tumor Antigens Occurs in a Specialized Environment of the Spleen, Cell Reports (2012), http://dx.doi.org/10.1016/j.celrep.2012.08.006

Cell PRESS
Open ACCESS

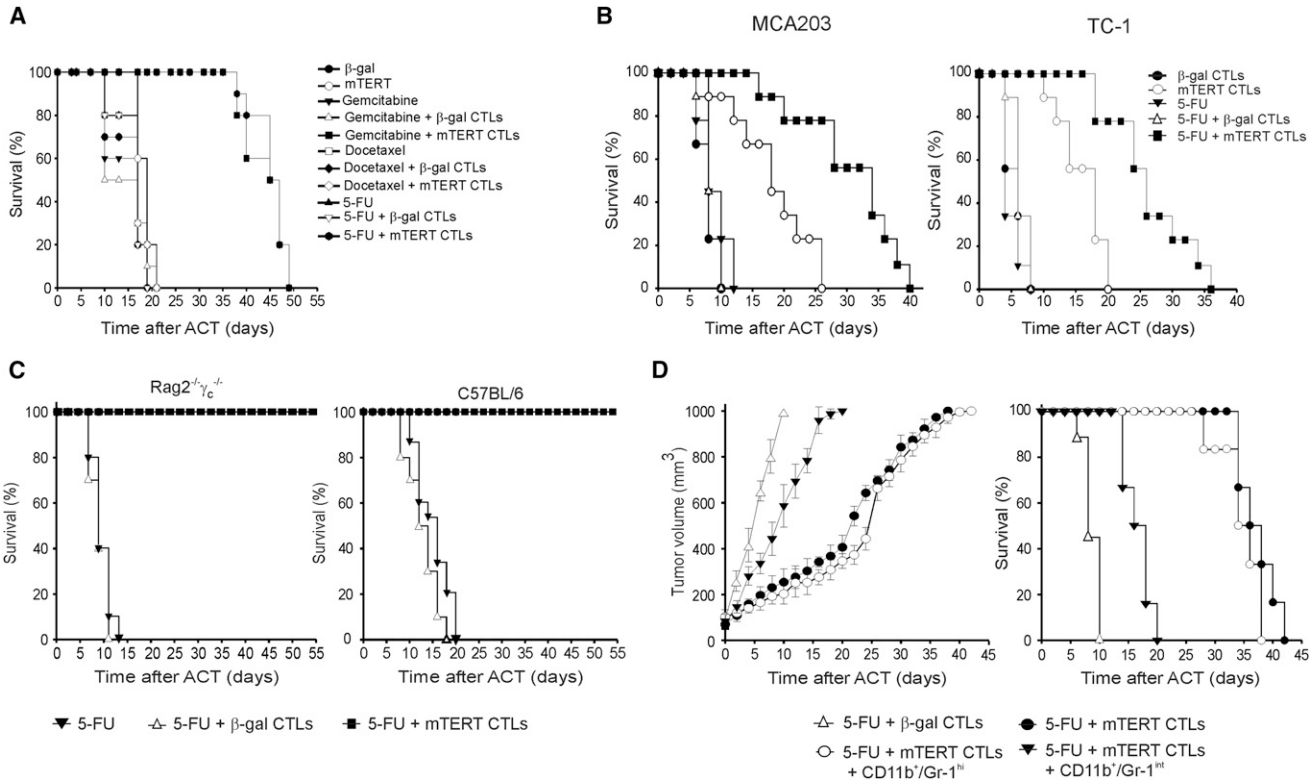

Figure 2. Adjuvant Activity of Low-Dose Chemotherapy on Adoptive Immunotherapy

(A) Therapeutic effectiveness of a single combination of chemotherapy and ACT with $mTERT_{198-205}$ CTLs. C57BL/6 mice were injected with 10^6 MCA203 sarcoma cells in the right flank. When tumor volume was ~200 mm^3, mice were treated with a single i.p. injection of either 5-FU (40 mg/kg), gemcitabine (120 mg/kg), or docetaxel (10 mg/kg). After 3 days, mice received 5 × 10^6 CTLs i.v. Mice were sacrificed when tumor volume reached 1,000 mm^3. Survival data for one representative experiment (n = 10 for each group) are shown. Kaplan-Meier survival analysis: $mTERT_{198-205}$ CTLs versus $\beta\text{-gal}_{96-103}$ CTLs, p = 0.558; mTERT198-205 CTLs versus gemcitabine, p = 0.476; $mTERT_{198-205}$ CTLs versus docetaxel, p = 0.998; $mTERT_{198-205}$ CTLs versus 5-FU, p = 0.999; $mTERT_{198-205}$ CTLs versus $mTERT_{198-205}$ CTLs + gemcitabine, p = 0.0002; $mTERT_{198-205}$ CTLs versus $mTERT_{198-205}$ CTLs + docetaxel, p = 0.998; $mTERT_{198-205}$ CTLs versus $mTERT_{198-205}$ CTLs + 5-FU, p = 0.0002; $mTERT_{198-205}$ CTLs + 5-FU versus $mTERT_{198-205}$ CTLs + docetaxel, p = 0.0002; and $mTERT_{198-205}$ CTLs + 5-FU versus $mTERT_{198-205}$ CTLs + gemcitabine, p = 0.996.

(B) Therapeutic effectiveness of a single combination of 5-FU injection and ACT with $mTERT_{198-205}$ CTLs in different tumor models. *Rag2*$^{-/-}\gamma_c^{-/-}$mice were s.c. implanted with 10^6 of either TC-1 lung carcinoma or MCA203 sarcoma cells in the right flank. When tumor volume was ~200 mm^3, mice were treated as described in (A). Cumulative data from three separate experiments (n = 15/group) are shown. Kaplan-Meier survival analysis in MCA203 model: $mTERT_{198-205}$ CTLs versus $\beta\text{-gal}_{96-103}$ CTLs, p = 0.0031; $mTERT_{198-205}$ CTLs versus 5-FU, p = 0.0028; and $mTERT_{198-205}$ CTLs versus $mTERT_{198-205}$ CTLs + 5-FU, p = 0.0008. Mantel-Haenszel statistic analysis in TC-1 model: $mTERT_{198-205}$ CTLs versus $\beta\text{-gal}_{96-103}$ CTLs, p = 0.0049; $mTERT_{198-205}$ CTLs versus 5-FU, p = 0.0047; and $mTERT_{198-205}$ CTLs versus 5-FU + $mTERT_{198-205}$ CTLs, p = 0.0017.

(C) Therapeutic effectiveness of repeated combination of ACT and 5-FU every 15 days. *Rag-2*$^{-/-}\gamma_c^{-/-}$mice (left panel) and C57BL/6 mice (right panel) were implanted with MCA203 sarcoma cells and treated with 5-FU as described in (A). After 3 days, mice received ACT. Treatment was repeated on days 15, 30, and 45 following the first ACT. A survival plot derived from three separate experiments (n = 15 for each group) is shown. Kaplan-Meier survival analysis for *Rag2*$^{-/-}\gamma_c^{-/-}$ model: 5-FU + $mTERT_{198-205}$ CTLs versus 5-FU + $\beta\text{-gal}_{96-103}$ CTLs, p = 0.000012. Kaplan-Meier survival analysis for C57BL/6 mice model: 5-FU + $mTERT_{198-205}$ CTLs versus 5-FU + $\beta\text{-gal}_{96-103}$ CTLs, p = 0.000036.

(D) *Rag2*$^{-/-}\gamma_c^{-/-}$mice were implanted with MCA203 sarcoma cells and treated with 5-FU as described in (A). After 2 days, 5 × 10^6 $CD11b^+Gr\text{-}1^{int}$ or $CD11b^+Gr\text{-}1^{hi}$ cells, isolated from the spleen of MCA203 tumor-bearing *Rag2*$^{-/-}\gamma_c^{-/-}$ mice, were injected i.v. After 1 day, mice received $mTERT_{198-205}$ CTLs. A survival plot of one representative experiment (n = 6 for each group) is shown. Mantel-Haenszel statistic analysis: 5-FU + $mTERT_{198-205}$ CTLs versus 5-FU + $mTERT_{198-205}$ CTLs + $CD11b^+Gr\text{-}1^{int}$, p = 0.000557; 5-FU + $mTERT_{198-205}$ CTLs + $CD11b^+Gr\text{-}1^{int}$ versus 5-FU + $mTERT_{198-205}$ CTLs + $CD11b^+Gr\text{-}1^{hi}$, p = 0.000568; and 5-FU + $mTERT_{198-205}$ CTLs versus 5-FU + $mTERT_{198-205}$ CTLs + $CD11b^+Gr\text{-}1^{hi}$, p = 0.490.

See also Figure S2.

increased in the spleen but not in the bone marrow (Figure 3B, left panel). Moreover, a 2 hr BrdU pulse revealed that a fraction of $CD11b^+Gr\text{-}1^{int}$ and $CD11b^+Gr\text{-}1^{lo}$ cells was already proliferating within the spleen of tumor-bearing mice at this early time point (Figure 3B, right panel). Thus, it is likely that the chemotherapeutic drugs found to share immune adjuvant properties in our initial screening are effective in reducing the expansion of highly cycling myeloid cells. As expected, 5-FU reduced proliferation of all the cell subsets when it was given 24–48 hr prior to the BrdU pulse (data not shown); however, even if 5-FU given 28 days earlier strongly affected the $CD11b^+Gr\text{-}1^{int}$ cell numbers (Figure 3A), the percentage of $BrdU^+$ cells in 5-FU treated animals

Cell PRESS
Open ACCESS

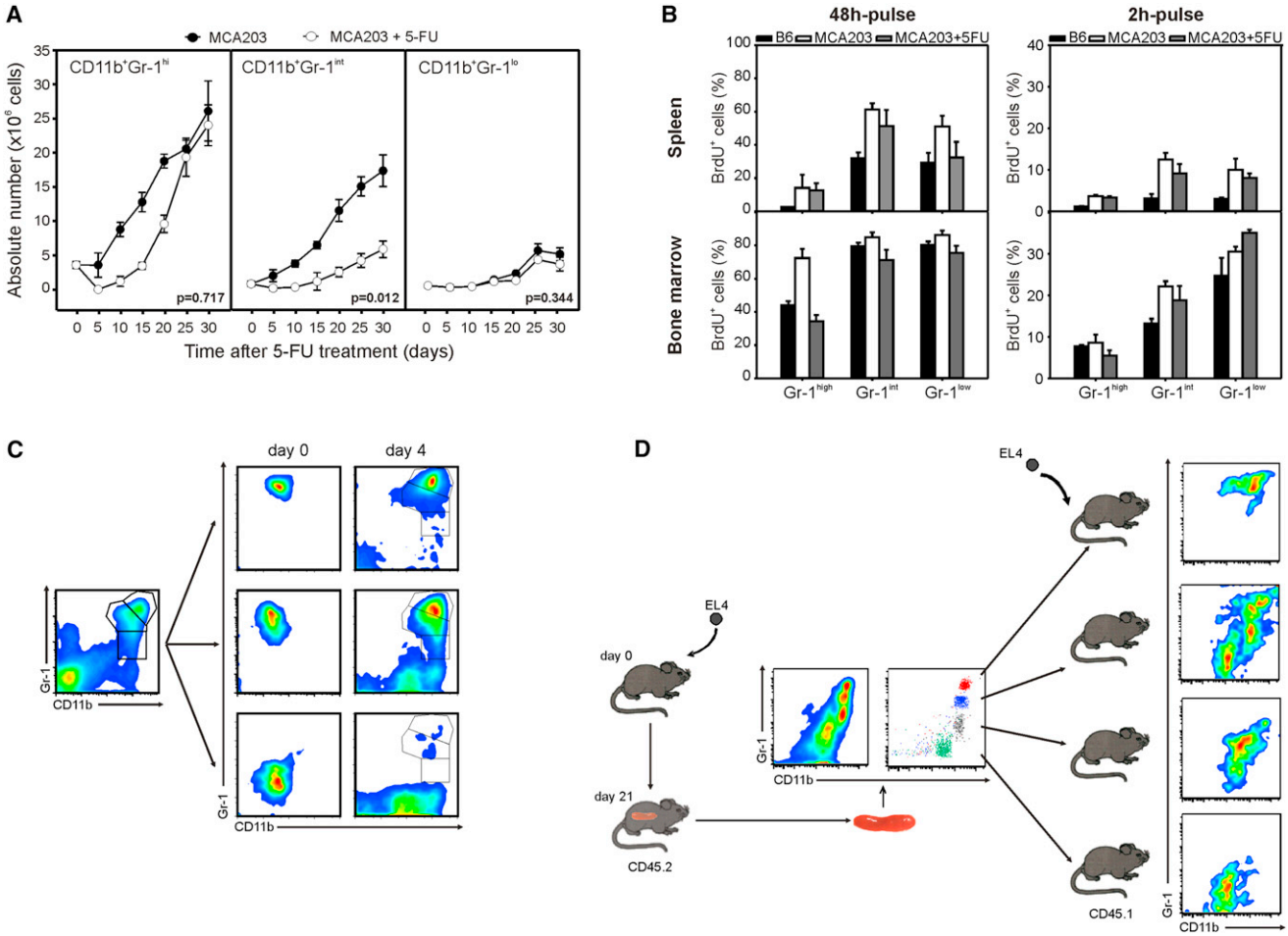

Figure 3. CD11b$^+$Gr-1^{int} Cells Comprise Highly Proliferating Myeloid Progenitors

(A) Kinetics of spleen repopulation of CD11b$^+$Gr-1^{hi}, CD11b$^+$Gr-1^{int} and CD11b$^+$Gr-1^{lo} cells after either 5-FU or PBS treatment. C57BL/6 mice were s.c. injected with 1 × 10^6 MCA203 sarcoma cells in the right flank. After 3 hr, they were treated with a single dose of 5-FU. Mice were sacrificed at different times after chemotherapy. Data are represented as mean ± SD (n = 3 mice) for each time point. Student's t test is reported for day 30.

(B) Proliferative potential of myeloid cell subsets in either spleen (upper panels) or bone marrow (lower panels) was assessed by means of BrdU incorporation, evaluated 48 hr (left panels) or 2 hr (right panels) after its in vivo inoculation. Data are represented as mean ± SE (n = 3 mice) of one representative experiment out of two independently performed experiments.

(C) Splenic CD11b$^+$ cells were FACS-sorted from the spleen of tumor-bearing mice and cultured for 4 days with GM-CSF (40 ng/ml) and IL-6 (40 ng/ml). Representative dot-plot of one of three independent experiments.

(D) Adult CD45.2 C57BL/6 mice were injected with 1 × 10^6 syngeneic EL4 mouse thymoma cells. CD11b$^+$Gr-1^{hi}, CD11b$^+$Gr-1^{int}, CD11b$^+$Gr-1^{lo}, and CD11b$^+$Gr-1$^-$ cells were FACS-sorted from the spleens of tumor-bearing mice 2 weeks following implantation. Then 1 × 10^6 sorted cells were adoptively transferred to adult CD45.1 C57BL/6 mice that had been implanted 1 week before with 1 × 10^6 EL4 cells. The phenotype of CD45.2 cells was analyzed 7 days after adoptive transfer by flow cytometry. Representative dot-plots (n = 4 mice/group).

See also Figure S3.

was not significantly altered within this cell population at such a late time point (Figure 3B), suggesting that the few CD11b$^+$ Gr-1^{int} cells conserved their proliferative activity.

Proliferating hematopoietic stem cells and granulocyte/macrophage progenitors were recently shown to accumulate in the spleen of tumor-bearing mice (Cortez-Retamozo et al., 2012). However, these progenitors do not express lineage markers such as CD11b and Gr-1. Thus, we considered the possibility that tumors could also cause the splenic expansion of committed precursors with high proliferative potential.

Purified splenic CD11b$^+$Gr-1^{int} cells are phenotypically homogeneous (i.e., they all express Ly6C and F4/80 monocyte/macrophage markers), bear morphological features of both immature myeloid cells (i.e., doughnut nuclei and CD117 expression; Biermann et al., 1999; Ogawa et al., 1991) and Ly6C^{hi}CCR2$^+$ inflammatory monocytes (Geissmann et al., 2003), and strongly suppress Ag-activated T lymphocytes (Figures S3Aand S3B). To test the potential of this cell fraction to reconstitute the myeloid descendants, we isolated CD11b$^+$Gr-1^{hi}, CD11b$^+$Gr-1^{int} and CD11b$^+$Gr-1^{lo} cells from the spleens of tumor-bearing mice and

Please cite this article in press as: Ugel et al., Immune Tolerance to Tumor Antigens Occurs in a Specialized Environment of the Spleen, Cell Reports (2012), http://dx.doi.org/10.1016/j.celrep.2012.08.006

Cell PRESS
Open ACCESS

cultured them with a combination of GM-CSF and IL-6, which we previously demonstrated to be sufficient to generate in vitro myeloid suppressors from bone marrow cells (Marigo et al., 2010; Sonda et al., 2011). As shown in Figure 3C, only the CD11b$^+$Gr-1^{int} fraction was able to give rise to all the other CD11b$^+$ myeloid subsets. Of more importance, when we followed the fate of the same splenic cell subsets in vivo by using congenic markers, after injection into tumor-bearing recipients, only CD11b$^+$Gr-1^{int} cells displayed the broadest spectrum of myeloid cell differentiation (Figure 3D). The same behavior could also be observed when cells were transferred to and traced in tumor-free mice (Figure S3C). Moreover, when CD11b$^+$Gr-1^{hi}, CD11b$^+$Gr-1^{int}, and CD11b$^+$Gr-1^{lo} subsets were tested in a colony-forming unit (CFU) assay, small round colonies, mainly resembling CFU-M, could be detected only in CD11b$^+$Gr-1^{int} agar cultures (Figure S3D). These observations led us to conclude that splenic CD11b$^+$Gr-1^{int} cells comprise a specific population of inflammatory monocytes with multipotent progenitor features that, although partially committed, may contribute to myeloid replenishment in the spleen during tumor growth.

A Tolerogenic Environment in the Marginal Zone of the Spleen of Tumor-Bearing Hosts

When we performed immunostaining of the spleens for CD19 (lymphoid follicles rich in B cells), CD8 (T cell areas of white pulp), and Ly6C (as a marker of CD11b$^+$Gr-1^{int} cells; Figure S4A), we noticed that Ly6C^{hi} myeloid cells were mostly distributed within the marginal zone (MZ) and the outer layers of lymphoid follicles (Figures S4A and S4B), which have been described as the transit areas for memory CD8$^+$ T cells during response to infection (Khanna et al., 2007). The tumor induced an expansion of Ly6C$^+$ cells in the MZ, which appeared hyperplastic (Figure S4B, lower panel). Indeed, although B cell follicles accounted for almost half of the spleen in tumor-free mice, their relative area was strongly reduced in the spleens of tumor-bearing mice, due to the accumulation of myeloid cells (Figure 4A). 5-FU administration reestablished a normal cytoarchitecture in the spleens of tumor-bearing hosts by reducing myeloid cell expansion and consequently MZ hyperplasia. A cytofluorimetric analysis of CD11b$^+$Gr-1$^+$ splenocytes confirmed the differences observed by confocal microscopy (Figure 4B; Figure S4C).

Given the relevance of the CCR2 receptor in the inflammatory monocyte egress from bone marrow and recruitment to peripheral tissues under several pathological conditions, including tumor growth (Lesokhin et al., 2011, 2012; Leuschner et al., 2011; Shi and Pamer, 2011), we speculated that it might also play a role in the accumulation of Ly6C$^+$ cells in the MZ of the spleen. Of interest, when we analyzed spleen sections from *Ccr2*$^{-/-}$ and *Ccl2*$^{-/-}$ mice, we observed a normal cytoarchitecture and reduced myeloid accumulation despite the presence of the tumor (Figures 4A and 4B; Figures S4B and S4C). CCR2 and CCL2 knockout phenocopied 5-FU treatment in terms of both myeloid subset reduction and the ability to completely abrogate the immunosuppressive influence exerted by the splenic environment on Ag-specific CD8$^+$ T lymphocyte proliferation (Figure 4C).

Spontaneous CCL2 production by whole splenocytes is strongly increased in tumor-bearing mice, and isolated CD11b$^+$ cells clearly participate in the increase in chemokine production, likely creating a positive feedback loop that enhances monocyte recruitment to this organ (Figure 4D). Nestin-positive bone marrow mesenchymal stem cells were recently shown to release CCL2 rapidly in response to circulating toll-like receptor ligands or bacterial infection, and cause inflammatory monocyte trafficking from the bone marrow into the bloodstream (Shi et al., 2011). In addition to myeloid Ly6C$^+$ cells (Figure S4D), Nestin$^+$ splenocytes (but not CD31$^+$ endothelial cells) also express CCL2 in the spleen of tumor-bearing hosts, as shown in Figure 4E and Figure S4E. These cells were rarely detectable in the spleen of tumor-free mice (not shown).

Splenic Immature Monocytes Cross-Present Tumor Ag and Tolerize CD8$^+$ T Lymphocytes

The relevant expansion of CD11b$^+$Gr-1^{int}Ly6C^{hi} cells in the spleen makes a direct interplay with CD8$^+$ T cells highly probable, and indeed, recurrent contacts between these two cell types were observed. In particular, we noticed that Ly6C$^+$CD8$^+$ T cells, which display a CD62L$^+$CD44$^+$CD127$^+$CD25$^-$ T central memory phenotype (T_{CM}) and a strong cytotoxic activity (Figure S5A), are preferentially surrounded by Ly6C$^+$ (monocytes) rather than Ly6G$^+$ (granulocytes) cells, in contrast to Ly6C$^-$CD8$^+$ naïve T lymphocytes (Figures 5A–5E; Figures S5B and S5C). Memory CD8$^+$ T lymphocytes could also be tracked as CD11b$^-$Gr-1^{int}Ly6C^{hi} cells (Figure S5A; in these CD8$^+$ T lymphocytes, Gr-1 expression is entirely due to the presence of the Ly6C), and their percentages in the spleen were inversely related to the percentages of CD11b$^+$Gr-1^{int}Ly6C^{hi} monocytes during tumor development (Figures S2C, S2D and, S5D), suggesting that these two cell types may interfere with each other for spleen occupancy. We speculated that the prolonged and selective loss of CD11b$^+$Gr-1^{int}Ly6C^{hi} cells in the spleen following 5-FU treatment (Figure 3A) could be explained by the occupancy of the MZ by drug-resistant Ly6C$^+$Gr-1^{int}CD8$^+$ T cells, which are poorly proliferating (Figure S5E) and thus are not likely affected by a low-dose chemotherapy. Indeed, in *Rag2*$^{-/-}\gamma_c^{-/-}$ immunodeficient mice, which lack B and T lymphocytes, myeloid cell subsets were largely unaffected 30 days after 5-FU treatment, in comparison with wild-type littermates (Figures S5F and S5G). Moreover, when Ly6C$^+$Gr-1^{int}CD8$^+$ T cells, but not CD4$^+$ and Ly6C$^-$CD8$^+$ (naïve) T cells, were transferred to tumor-bearing *Rag2*$^{-/-}\gamma_c^{-/-}$ recipients following low-dose chemotherapy, the myeloid cell numbers were significantly reduced, highlighting the role of memory CD8$^+$ T lymphocytes in hampering myeloid expansion and spleen replenishment (Figure 5F).

It has been suggested that splenic CD11b$^+$Gr-1$^+$ cells can process and present tumor Ags (Kusmartsev et al., 2005). We hypothesized that contacts between CD11b$^+$Ly6C^{hi} cells and memory CD8$^+$ T lymphocytes in the spleen could result in the direct cross-presentation of tumor Ags in a tolerogenic manner. Indeed, splenic CD11b$^+$ cells isolated from OVA-EG7 tumor-bearing mice initially primed OVA-specific CD8$^+$ T lymphocytes to proliferate in the absence of the exogenous peptide (Figure 5G, left panel), whereas CD11b$^+$ splenocytes from mice bearing the same tumor lacking OVA Ag (EL4) were inactive, indicating that the proper OVA peptide was processed and presented. However, after the first stimulation by CD11b$^+$ cells,

Cell PRESS
Open ACCESS

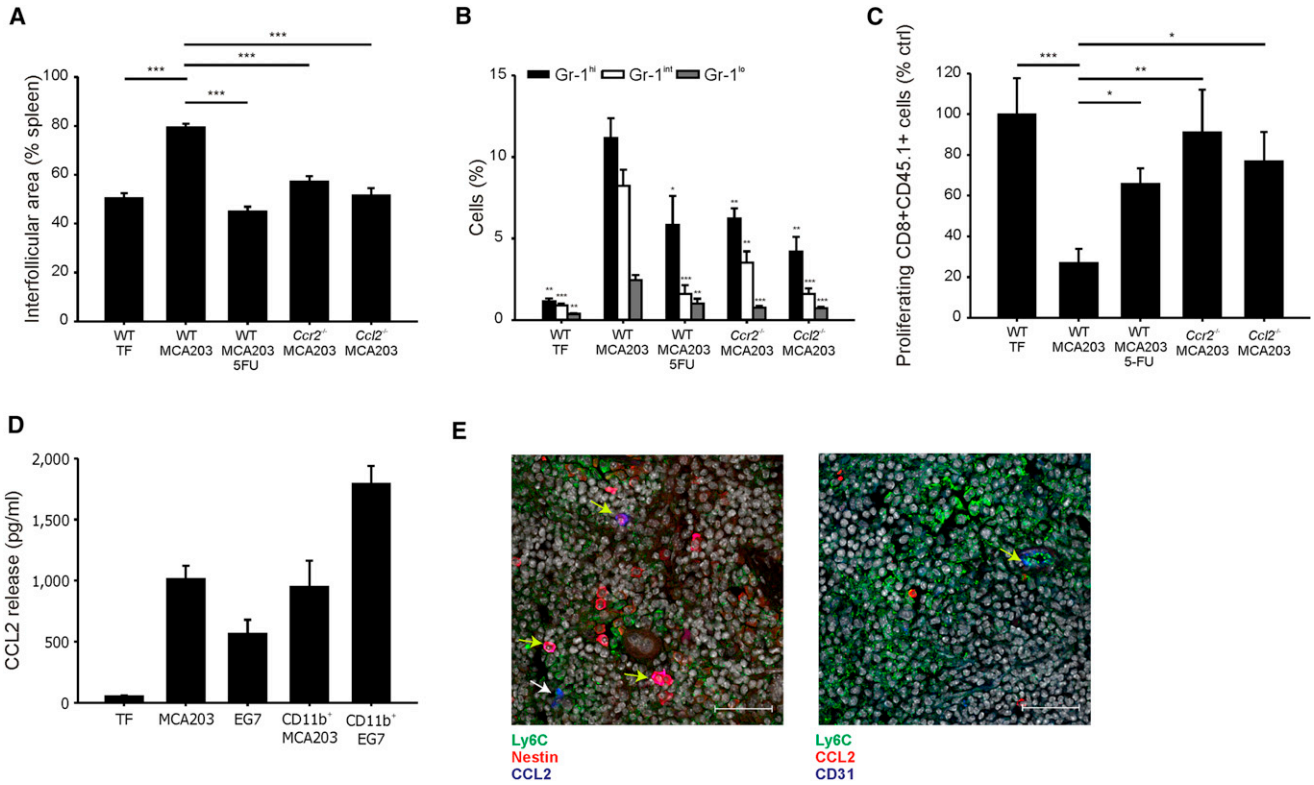

Figure 4. The CCL2/CCR2 Axis Is Crucial for CD11b$^+$Gr-1^{int}Ly6C^{hi} Monocyte Recruitment to the Spleen

(A) Interfollicular area was calculated as the percentage of the whole spleen section by collecting 30 images from at least three different MCA203-bearing mice for each of the indicated groups. Mean ± SD.

(B) Splenic distribution of myeloid subsets, determined by FACS staining of splenocytes for CD11b and Gr-1 markers in tumor-free and MCA203 tumor-bearing mice from the indicated groups. Tumor-bearing mice were sacrificed 25 days after tumor injection. Data represent mean ± SE of three separate experiments (n = 4 mice/group for each experiment). Comparisons among myeloid subsets from either tumor-free or MCA203 tumor-bearing mice were performed with Student's t test.

(C) CFSE-labeled, OVA-specific CD8$^+$ T cells were cultured in the presence of splenocytes from the indicated experimental groups. Proliferation was compared and normalized to MLPC setup with splenocytes from tumor-free mice. Data represent mean ± SE of three independent experiments (n = 3 mice/group for each experiment). Statistical analysis was performed with Student's t test.

(D) CCL2 release was measured in the supernatants of 48 hr cultures of either total or CD11b$^+$-sorted splenocytes, isolated from either tumor-free or (MCA203, EG7) tumor-bearing mice, by ELISA. Data are presented as mean ± SE of three independent experiments.

(E) Immunofluorescence was performed on thin spleen cryosections from MCA203 tumor-bearing mice. Scale bars are 50 μm. In the left panel, yellow arrows point to Nestin$^+$CCL2$^+$ cells and white arrows point to Ly6C$^+$CCL2$^+$ cells. In the right panel, arrowheads point to CD31$^+$CCL2$^-$ cells.

See also Figure S4.

the same OVA-specific T lymphocytes were no longer able to respond to the cognate Ag upon restimulation with the Ag presented by Ag-presenting cells (Figure 5G, right panel). We observed that cross-presentation and tolerance induction involved, at least partially, the uptake of tumor Ags from blood circulating exosomes, as the exosome inhibitor dimethyl-amiloride (DMA) (Chalmin et al., 2010) was shown to limit the extent of both cross-presentation and tolerance when administered in vivo to tumor-bearing mice. Intriguingly, Ag cross-presentation and consequently cross-tolerance were abrogated in *Ccr2*$^{-/-}$ mice, indicating that splenic CD11b$^+$CCR2$^+$ myeloid cells are responsible for cross-tolerization of peripheral CTLs (Figure 5G). This functional behavior was fully mirrored by the ability of splenic CD11b$^+$ cells to cross-present tumor-derived OVA peptide on MHC I class molecules on their surface, since either DMA treatment or CCR2 deficiency strongly impaired Ag presentation (Figure 5H). CD11b$^+$Gr-1^{int}Ly6C^{hi}CCR2$^+$ monocytes positive for MHC I-OVA peptide complexes were also detected among tumor-infiltrating leukocytes, but were not observed in tumor-draining lymph nodes, bone marrow, or blood (data not shown). The splenectomy experiments described above thus indicate that even if tumor Ag presentation occurs within the tumor environment, it is not sufficient to induce Ag-specific tolerance.

CCL2 Serum Levels Are Predictive of the Clinical Outcome in Patients Responding to Cancer Vaccination

Using *Ccl2*$^{-/-}$ mice, we noticed that CCL2 deficiency helped the endogenous immune response to eradicate tumor cells exclusively when mice were implanted with highly antigenic tumor cells, as in the case of 4T1-HA mammary carcinoma (Figure 6A). To investigate whether this observation could be relevant for clinical purposes, we assessed CCL2 serum levels in patients

Cell PRESS
Open ACCESS

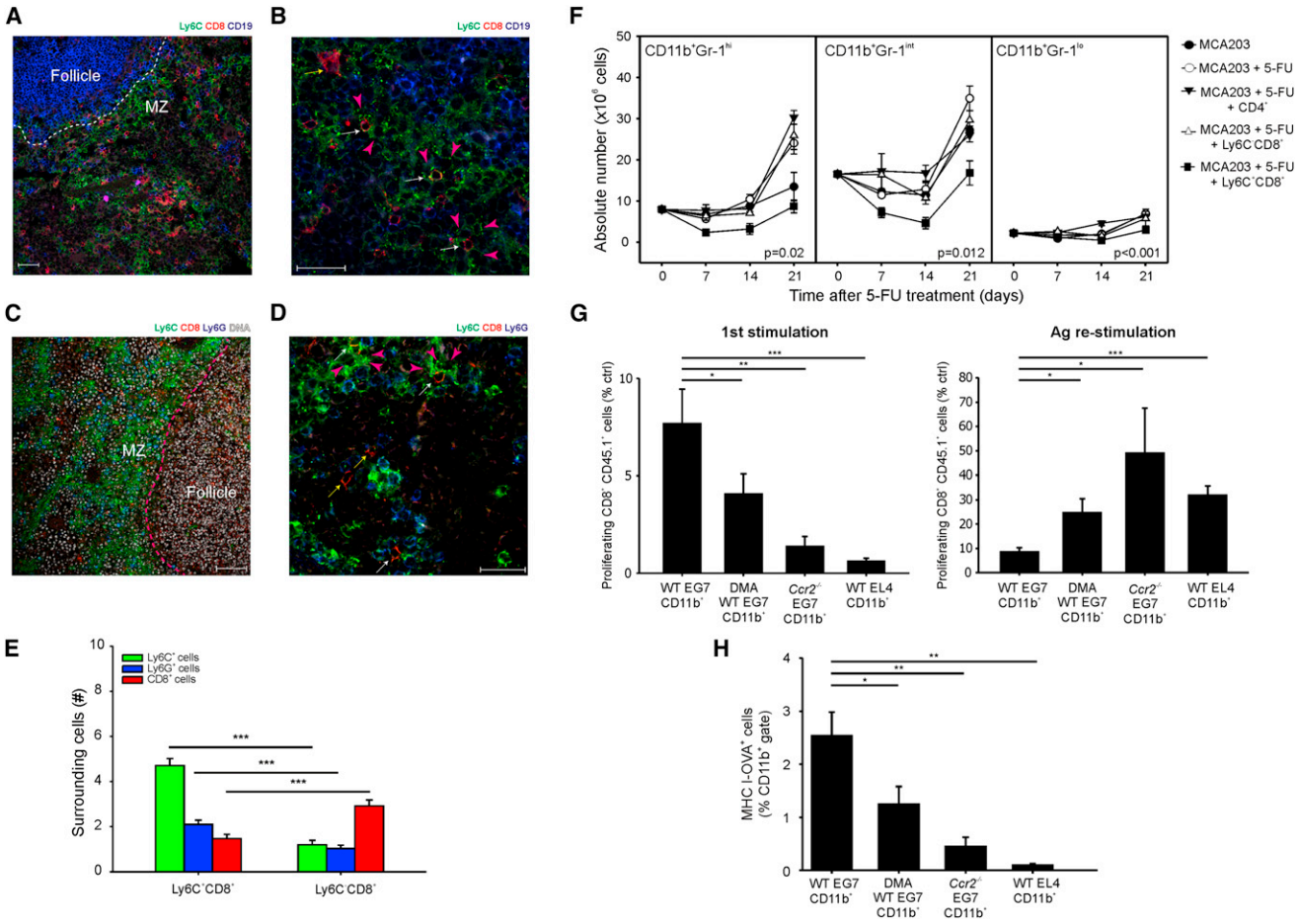

Figure 5. Splenic CD11b$^+$Ly6C^{hi} Monocytes Are in Close Contact with and Cross-Present Tumor Ags to CD8$^+$ T Cells

(A–D) Distribution of Ly6C$^+$CD8$^+$ (memory T lymphocytes), Ly6C$^+$CD8$^-$ (monocytes), and Ly6C$^-$CD8$^+$ (naïve T lymphocytes) cells in the spleen of MCA203 tumor-bearing mice. White arrows point to Ly6C$^+$CD8$^+$ cells, yellow arrows point to Ly6C$^+$CD8$^-$ cells, and pink arrowheads point to Ly6C$^+$ myeloid cells. Scale bars are 50 μm for (A) and (C), and 25 μm for (B) and (D).

(E) The numbers of Ly6C$^+$Ly6G$^-$CD8$^-$ (green bars), Ly6C$^{+/-}$Ly6G$^+$CD8$^-$ (blue bars), and Ly6C$^-$Ly6G$^-$CD8$^+$ (red bars) cells surrounding either Ly6C$^+$CD8$^+$ or Ly6C$^-$CD8$^+$ lymphocytes were calculated as described in Figure S5B. Data are presented as mean ± SE (n = 70 cells/group). Statistical analysis was performed with Student's t test.

(F) *Rag2*$^{-/-}\gamma_c^{-/-}$ mice were s.c. implanted with MCA203 sarcoma cells and after 3 hr were treated with a single dose of 5-FU. After 2 days, 10^6 of CD8$^+$Ly6C$^+$, CD8$^+$Ly6C$^-$, or CD4$^+$ T cells were injected i.v. in the same mice. *Rag2*$^{-/-}\gamma_c^{-/-}$ mice were sacrificed at different time points after chemotherapeutic treatment. Statistical analysis was performed with Student's t test; p values for the comparison between MCA203 + 5-FU and MCA203 + 5FU + CD8$^+$Ly6C$^+$ groups on day 21 are shown.

(G) CD11b$^+$ cells were isolated from the spleen of either wild-type or *Ccr2*$^{-/-}$ EG7 or EL4 tumor-bearing mice and cultured for 3 days together with CFSE-labeled, OVA-specific CD8$^+$ T cells (left panel) in the absence of exogenous peptide. The values reported refer to cultures with 24% CD11b$^+$ cells on total cell counts. When required, mice received daily i.p. injection of DMA for 1 week before sacrifice. OVA-specific CD8$^+$ T cell proliferation, measured by CFSE dilution, was normalized to the values obtained in the presence of OVA peptide-pulsed feeder cells (ctrl). Lymphocytes from the former cultures were restimulated with Ag-pulsed feeder cells (right panel), and CFSE dilution was measured 3 days after the second stimulation. OVA-specific CD8$^+$ T cell proliferation was normalized to the values obtained in control cultures. Data represent mean ± SE of three independent experiments (n = 3 mice/group for each experiment). Statistical analysis for the indicated comparisons was performed with Student's t test.

(H) MHC class I-OVA complexes were labeled on splenic CD11b$^+$ cells used in the previous cultures. Data represent mean ± SE of three independent experiments (n = 3 mice/group for each experiment). Statistical analysis for the indicated comparisons was performed with Student's t test.

See also Figure S5.

who had undergone active immunotherapy. We considered patients with renal cell carcinoma (RCC) and colorectal cancer (CRC) who were enrolled in phase I/II studies and had received two therapeutic vaccines, IMA901 and IMA910, respectively, which consist of naturally presented tumor-associated peptides (TUMAPs; Walter et al., 2012). In these trials, CCL2 serum levels measured prior to vaccination were used to classify the patients into subgroups with respect to their OS. There was no difference in the number of multipeptide immune responders versus nonresponders among patients with either low or high CCL2 serum

Cell PRESS
Open ACCESS

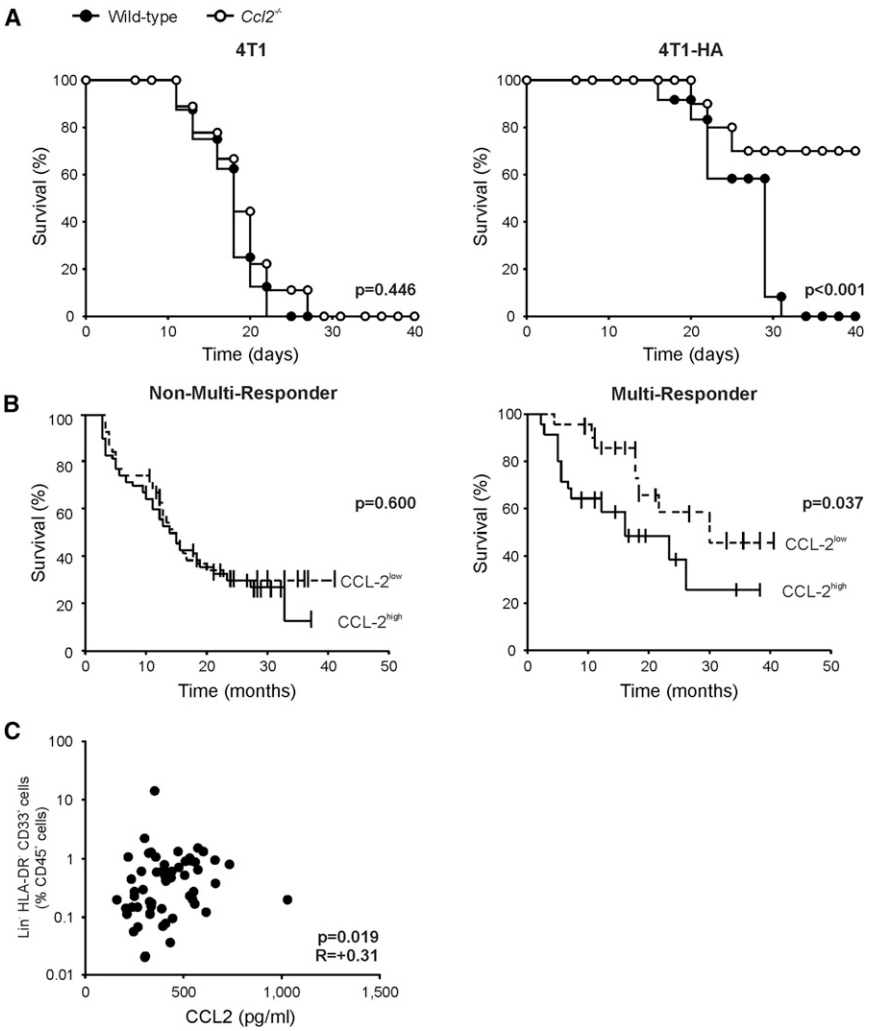

Figure 6. CCL2 Serum Levels Correlate with Myeloid Cell Accumulation and Response to Immunotherapy in Renal Cell and Colorectal Cancer Patients

(A) BALB/c (left panel) or *Ccl2*$^{-/-}$ (right panel) mice were subcutaneously injected with either 4T1 or 4T1-HA cell lines. Mice survival (n = 12 mice/group) was analyzed by means of the Kaplan-Meier method.

(B) Combined analysis of OS in RCC and CRC patients who were evaluable for immune and CCL2 analyses, were enrolled in an immunotherapy phase I/II study, and had received multipeptide vaccines. Shown is a survival plot of patients without (left panel, n = 88) or with (right panel, n = 48) vaccine-induced multipeptide responses, grouped by CCL2 levels above (solid line) or below (dashed line) the median value.

(C) Spearman's rank correlation analysis of serum CCL2 and Lin$^-$HLA-DR$^-$CD33$^+$ myeloid cell levels among PBMCs, determined prior to immunotherapy, in individual RCC patients (· represents individual patients, n = 58).

See also Figure S6 and Table S1.

levels. In agreement with our preclinical results, however, only in patients who developed multiple T cell responses to peptide vaccination were high CCL2 serum levels predictive of worse prognosis in terms of OS (Figure 6B). Pretreatment levels of distinct subsets of myeloid cells were significantly increased in the blood of these patients relative to healthy controls (Walter et al., 2012). Of interest, we observed that, at least in the patients with RCC, CCL2 serum levels directly correlated with peripheral blood mononuclear cell (PBMC) frequencies in an immature Lin$^-$HLA-DR$^-$CD33$^+$ myeloid cell subset (Figure 6C), which was recently described as highly proliferating, strongly immunosuppressive, and predictive of disease progression in CRC and breast cancer (Solito et al., 2011). Correlations of pretreatment CCL2 serum levels with other human myelomonocytic cell subsets were less robust (Figure S6; Table S1).

DISCUSSION

It has recently become clear that the immune system has a crucial role in modulating tumor progression and response to therapy. Numerous anticancer agents that were used in the past for their cytotoxic properties can modulate the host immune system, and sometimes induce a long-term protective memory T cell response. We unveiled a previously unknown environment in the MZ of the spleen of tumor-bearing hosts in which immunoregulatory monocytes coexist with memory CD8$^+$ T cells. These multipotent inflammatory monocytes are recruited to the MZ by CCL2 and cross-tolerize Ag-specific lymphocytes, at least in part by sampling tumor-released exosomes. Because of the high proliferative rate of these monocytes, some chemotherapeutic agents are very active in depleting them while sparing poorly proliferating lymphocytes, and the subsequent occupation of the splenic environment by CD8$^+$ T cells hampers the replenishment of myeloid cells following chemotherapy. The contribution of both depletion of regulatory T lymphocytes and induction of immunogenic cancer cell death by chemotherapy to the described phenomena was negligible. These findings provide a rational explanation for the often empirical and paradoxical observation that chemotherapy is one of the most effective adjuvants for ACT, and suggest that an extensive lympho-myeloablation before ACT is likely unnecessary or even detrimental. We propose that our findings lay the foundation for defining both the dose and class of chemotherapeutic agents that will have the greatest impact on ACT.

Our data depict two scenarios for future approaches aimed at enhancing ACT therapeutic impact. First, metronomic chemotherapy treatment could be exploited to maintain a long-term contraction of the immunosuppressive monocyte expansion. Metronomic chemotherapy was originally developed to

Cell PRESS
Open ACCESS

overcome drug resistance; however, low-dose cyclophosphomide was reported to limit regulatory T lymphocytes and increase innate immune response (Ghiringhelli et al., 2004; Ghiringhelli et al., 2007). Second, chemotherapeutic drugs with distinct immunomodulatory properties could be combined with cancer immunotherapy. As recently reviewed, in fact, some agents can induce immunogenic cancer-cell death (Galluzzi et al., 2012; Zitvogel et al., 2011). Of interest, many of the drugs that alter the splenic immunoregulatory environment do not affect the immunogenic context of cancer death. Future developments could thus be based on optimizing low-dose chemotherapy to eliminate immunosuppressive monocytes before administering a specific drug that is able to elicit immunogenic death and increase tumor-Ag uptake by APCs present in the tumor microenvironment.

A prediction based on our data is that adoptive transfer of Ag-specific $CD8^+$ T_{CM} would be the best choice for passive immunotherapy, because these cells may be able to interfere with myeloid cell expansion in the spleen following chemotherapy. Indeed, this hypothesis is supported by some published experimental data showing that adoptively transferred $CD8^+$ T_{CM} were more potent than effector memory $CD8^+$ T cells specific for a melanoma Ag in causing the eradication of large established tumors (Klebanoff et al., 2005). Of interest, this greater efficacy achieved with $CD8^+$ T_{CM} was related to the ability of tumor-reactive T cells to traffic better to secondary lymphoid organs than to tumor sites (Klebanoff et al., 2005).

In mouse studies, a relationship between the extent of lympho- and myelodepletion and the magnitude of the in vivo antitumor effect of the transferred cells seemed to emerge (Wrzesinski et al., 2010; Wrzesinski and Restifo, 2005). However, our data suggest that myeloablative chemotherapy may not be necessary for an optimal adjuvant activity of ACT. In the case of 5-FU, for example, relatively low doses of drugs were administered (40 mg/kg versus 100 mg/kg, which is commonly used in preconditioning regimens). On the basis of our data, we can hypothesize that high-dose chemotherapy can be either detrimental or beneficial depending on its prevailing effects on the myeloid or lymphoid compartment.

CCL2 has multiple roles in cancer progression. $Gr\text{-}1^+$ inflammatory monocytes were not found at primary mammary tumor lesions, and instead were preferentially recruited by CCL2 to pulmonary metastases to assist tumor spreading. Moreover, CCL2 expression and macrophage infiltration were shown to correlate with poor prognosis and metastatic disease in human breast cancer (Qian et al., 2011). Recent evidence, however, shows that the antitumor effects of CCL2 blockade in vivo are dependent on the host immune system. In fact, administration of anti-CCL2 monoclonal antibody (mAb) induced tumor-specific $CD8^+$ T cell activation and expansion rather than a decrease in the number of tumor-associated macrophages (Fridlender et al., 2010, 2011). Moreover, the antitumor effects of CCL2 blockade was completely lost in immunodeficient mice or after $CD8^+$ T cell depletion, clearly enforcing the concept that CCL2 blockade reestablishes the immune response in the tumor-bearing host, in similarity to the data we obtained with either 5-FU administration or *ccl2*/*ccr2* gene knockout ablation. Moreover, we show here that CCL2 serum levels correlate with the expansion of immature myeloid cells in the blood of cancer patients, and, more importantly, with the clinical response to cancer vaccination in patients who develop broad immune responses to the tumor Ags present in the vaccine. The spleen is not easily accessible in patients, but our findings indicate that blood may be used to provide information relevant for the clinical outcomes of cancer immunotherapy.

EXPERIMENTAL PROCEDURES

Splenectomy

The abdominal cavity of mice under general anesthesia (Rompum and Zoletil) was opened and the spleen vessels were cauterized. The spleen was carefully removed and placed in cold phosphate-buffered saline (PBS) solution. For control experiments, the abdomen was opened but the spleen was not removed (sham surgery).

In Vivo Tolerance Assay

C57BL/6 mice were either splenectomized or subjected to sham surgery. After 10 days, 0.5×10^6 EG7 cells were injected subcutaneously (s.c.) into the flank of $CD45.2^+$ mice. Seven days later, the mice were adoptively transferred with 2×10^7 splenocytes derived from OT-1 transgenic mice ($CD45.1^+$), corresponding approximately to 5×10^6 OVA-specific $CD8^+$ T cells. Two weeks after tumor injection, the animals were euthanized and cells from lymph nodes and spleens were tested by ELISpot and intracytoplasmic cytokine staining (ICS) as previously described (Dolcetti et al., 2010a, 2010b; Marigo et al., 2010). Where indicated, tumor-bearing mice were s.c. vaccinated with 1×10^6 $OVA_{257\text{-}264}$ peptide-pulsed DCs 2 days post lymphocyte transfer (Dolcetti et al., 2010a). When Ag-experienced $CD8^+$ T cells were adoptively transferred, OT-1 splenocytes were cultured with the cognate peptide and 20 U/ml IL-2 for 5 days (>97% $CD8^+$ cells after stimulation). Similar experiments were performed on a BALB/c background, with s.c. injection of 1×10^6 4T1-HA tumor cells 10 days after surgery. After 20 days, the mice were transferred with 2×10^7 splenocytes derived from CL4 mice and were vaccinated with 1×10^6 $HA_{512\text{-}520}$-peptide pulsed DCs 2 days after ACT. The mice were sacrificed at day 26 and lymph nodes were stimulated as previously described.

ACT

ACT in mouse transplantable tumor models was performed in $Rag2^{-/-}\gamma_c^{-/-}$ and C57BL/6 mice after subcutaneous challenge with 1×10^6 tumor cells. When the tumor volume was ~200 mm^3, the mice were treated with 40 mg/kg 5-FU. After 3 days, 5×10^6 Ag-specific CTLs were intravenously (i.v.) injected. At the time of CTL transfer, mice were intramuscularly (i.m.) injected with 5×10^8 PFU of a recombinant adenoviral vector coding for the relevant Ag recognized by transferred T cells and then intraperitoneally (i.p.) treated with 30,000 IU rIL-2 twice a day for 3 consecutive days. Blind measurements of tumor mass were carried out with the use of digital calipers. Mice were euthanized when the tumor volume reached 1,000 mm^3. In some experiments, OVA-specific $CD8^+$ T cells were administered to EG7-bearing recipients, as described previously (Molon et al., 2011).

Cell Isolation

$CD11b^+Gr\text{-}1^{hi}$ and $CD11b^+Gr\text{-}1^{int}$ cells were isolated with the use of Miltenyi Biotec antibodies and microbeads as previously described (Dolcetti et al., 2010a, 2010b). The purity of cell populations was evaluated by flow cytometry and exceeded 90%. For fluorescence-activated cell sorting (FACS) sorting, splenocytes were labeled with PERCP-Cy5.5 anti-CD11b and APC anti-Gr-1 mAb, and sorted to >98% purity with a FACSAria (BD) flow cytometer.

Cytotoxicity Assay

After 5 days, the cultures were tested for the ability to lyse an allogenic target (MLR) or target cells pulsed with a specific peptide (MLPC) in a 5 hr ^{51}Cr-release assay as previously described (Dolcetti et al., 2010a).

In Vitro Cross-Tolerance Assay

To evaluate myeloid-induced tolerance, CD11b$^+$ cells were immunomagnetically sorted from the spleens of EG7- or EL4-bearing mice and cultured, ranging from 24% to 3% of the whole culture, together with C57BL/6 and carboxyfluorescein succinimidyl ester (CFSE)-pulsed 1% OVA-specific splenocytes. $OVA_{257-264}$ peptide was added only to control cultures. After 3 days, proliferation was assessed by CFSE dilution in half of the cultures, and CTLs were recovered from the remaining cultures and plated with peptide-pulsed splenocytes for another 3 days. After 6 days from the initial culture, CFSE dilution was assessed in restimulated CTLs to evaluate the induction of tolerance. When required, EG7-tumor-bearing mice received daily i.p. injection of 1 μmol/kg DMA (Sigma-Aldrich) for 1 week before they were sacrificed.

Phase II Study of IMA901 in Renal Cell Cancer

IMA901 (Walter et al., 2012) is a therapeutic cancer vaccine based on the selection of naturally presented TUMAPs (nine HLA-A*02 and one HLA-DR binding). In the multicenter phase II study IMA901-202, 68 HLA-A*02-positive patients (intent-to-treat [ITT] group) with advanced clear-cell type RCC and documented progression during or after standard first-line therapy were randomized 1:1 to receive up to 17 intradermal vaccinations of IMA901 over 9 months, together with 75 μg granulocyte-macrophage colony-stimulating factor (GM-CSF) plus/minus a single infusion of cyclophosphamide (CY; 300 mg/m^2) 3 days before the first vaccination. A total of 64 patients were treated per protocol (PP). Blood for PBMCs isolation was collected at day −3, 1, 15, 22, and 36 relative to the first vaccination. Blood for serum analysis was collected at day −3.

Phase I/II Study of IMA910 in Colorectal Cancer

IMA910 is a peptide-based vaccine consisting of 10 HLA-A*02 binding and three HLA-DR binding TUMAPs presented on colorectal tumors and overexpressed relative to healthy tissues. The multicenter clinical phase I/II study IMA910-101 enrolled 92 HLA-A*02 ITT patients with advanced/metastatic CRC who were at least clinically stable after 12 weeks of first-line oxaliplatin-based therapy. The patients were infused with a single dose of CY (300 mg/m^2) 3 days prior to first vaccination and thereafter were repeatedly immunized intradermally (up to 16 vaccinations over 8 months) with IMA910 in combination with GM-CSF (75 μg, cohort 1; n = 66) or, in a second cohort, with GM-CSF plus topically applied imiquimod (2 × 12.5 mg, cohort 2; n = 26) as an additional adjuvant. A total of 82 patients were treated PP. Blood for PBMC isolation was collected at days −3, 1, 8, 15, 22, 36, and 57 relative to the first vaccination. Blood for serum analysis was collected at days −42 to −4.

Both clinical studies (IMA901-202 and IMA910-101) were conducted in accordance with the Declaration of Helsinki, current International Conference on Harmonisation of Technical Requirements for Registration of Pharmaceuticals for Human Use (ICH) guidelines, and all applicable regulatory and ethical requirements. Approvals by the relevant Institutional Review Boards were given and all subjects provided written informed consent before study-related procedures were performed.

Statistics

A two-tailed Student's t test or Wilcoxon's test was used to compare data sets, with an α-level of 0.05 (in the figures, significance is indicated as * $p \leq 0.05$, ** $p \leq 0.01$, and *** $p \leq 0.001$). A Kaplan-Meier survival analysis was performed for the comparison of survival curves. An unpaired, two-sided Welch's t test was used to test the association of serum CCL2 levels with T cell responses in both clinical trials. Because CCL2 was measured using different assays in both trials, differences between RCC and CRC CCL2 serum values may be due to differences in serum levels between the two diseases, or to differences between the two assays. To assess the influence of CCL2 serum levels on OS in a combined analysis of RCC and CRC patients (PP populations), we dichotomized continuous serum levels within each tumor entity by cutting at the medians of the respective ITT populations (median CCL2 RCC 396.5 pg/ml, CRC 1196.6 pg/ml) and assigning every patient to the $CCL2^{low}$ or $CCL2^{high}$ subgroup. We performed OS analyses using R (GNU) programming language version 2.14.2 with the "coin" package. We conducted a stratified log-rank test to assess the difference in OS between $CCL2^{low}$ and $CCL2^{high}$ patients using surv_test. Each trial (RCC or CRC) was included as a stratification factor to calculate the p values within multipeptide-responders and nonmultipeptide responders (PP). The correlation between CCL2 and MDSC levels was analyzed with Spearman's rank correlation. Kaplan-Meier curves and correlation analyses were generated with GraphPad Prism 5 software.

SUPPLEMENTAL INFORMATION

Supplemental Information includes Extended Experimental Procedures, six figures, and one table and can be found with this article online at http://dx.doi.org/10.1016/j.celrep.2012.08.006.

LICENSING INFORMATION

This is an open-access article distributed under the terms of the Creative Commons Attribution-Noncommercial-No Derivative Works 3.0 Unported License (CC-BY-NC-ND; http://creativecommons.org/licenses/by-nc-nd/3.0/legalcode).

ACKNOWLEDGMENTS

We thank Arben Dedja, Serena Zilio, Martina Piccoli, Maurizio Buggio, and Barbara Molon for technical help and critical discussions. This work was supported by grants from the Italian Ministry of Health; Italian Ministry of Education, Universities, and Research; Italian Association for Cancer Research (AIRC, grants 6599 and 12182); and Fondazione Cassa di Risparmio di Verona, Vicenza, Belluno e Ancona. T.W. is co-founder and employee of and holds shares and stock options of Immatics Biotechnologies. S.W. is an employee of and holds stock options of Immatics Biotechnologies.

Received: January 24, 2012
Revised: July 9, 2012
Accepted: August 13, 2012
Published online: September 6, 2012

REFERENCES

Biermann, H., Pietz, B., Dreier, R., Schmid, K.W., Sorg, C., and Sunderkötter, C. (1999). Murine leukocytes with ring-shaped nuclei include granulocytes, monocytes, and their precursors. J. Leukoc. Biol. *65*, 217–231.

Bronte, V., Wang, M., Overwijk, W.W., Surman, D.R., Pericle, F., Rosenberg, S.A., and Restifo, N.P. (1998). Apoptotic death of CD8+ T lymphocytes after immunization: induction of a suppressive population of Mac-1+/Gr-1+ cells. J. Immunol. *161*, 5313–5320.

Bronte, V., Chappell, D.B., Apolloni, E., Cabrelle, A., Wang, M., Hwu, P., and Restifo, N.P. (1999). Unopposed production of granulocyte-macrophage colony-stimulating factor by tumors inhibits CD8+ T cell responses by dysregulating antigen-presenting cell maturation. J. Immunol. *162*, 5728–5737.

Chalmin, F., Ladoire, S., Mignot, G., Vincent, J., Bruchard, M., Remy-Martin, J.P., Boireau, W., Rouleau, A., Simon, B., Lanneau, D., et al. (2010). Membrane-associated Hsp72 from tumor-derived exosomes mediates STAT3-dependent immunosuppressive function of mouse and human myeloid-derived suppressor cells. J. Clin. Invest. *120*, 457–471.

Cortez-Retamozo, V., Etzrodt, M., Newton, A., Rauch, P.J., Chudnovskiy, A., Berger, C., Ryan, R.J., Iwamoto, Y., Marinelli, B., Gorbatov, R., et al. (2012). Origins of tumor-associated macrophages and neutrophils. Proc. Natl. Acad. Sci. USA *109*, 2491–2496.

Dolcetti, L., Peranzoni, E., and Bronte, V. (2010a). Measurement of myeloid cell immune suppressive activity. Curr. Protoc. Immunol. *Chapter 14*, Unit 14.17.

Dolcetti, L., Peranzoni, E., Ugel, S., Marigo, I., Fernandez Gomez, A., Mesa, C., Geilich, M., Winkels, G., Traggiai, E., Casati, A., et al. (2010b). Hierarchy of immunosuppressive strength among myeloid-derived suppressor cell subsets is determined by GM-CSF. Eur. J. Immunol. *40*, 22–35.

Fridlender, Z.G., Buchlis, G., Kapoor, V., Cheng, G., Sun, J., Singhal, S., Crisanti, M.C., Wang, L.C., Heitjan, D., Snyder, L.A., and Albelda, S.M. (2010). CCL2 blockade augments cancer immunotherapy. Cancer Res. *70*, 109–118.

Fridlender, Z.G., Kapoor, V., Buchlis, G., Cheng, G., Sun, J., Wang, L.C., Singhal, S., Snyder, L.A., and Albelda, S.M. (2011). Monocyte chemoattractant protein-1 blockade inhibits lung cancer tumor growth by altering macrophage phenotype and activating CD8+ cells. Am. J. Respir. Cell Mol. Biol. *44*, 230–237.

Gabrilovich, D.I., and Nagaraj, S. (2009). Myeloid-derived suppressor cells as regulators of the immune system. Nat. Rev. Immunol. *9*, 162–174.

Gabrilovich, D.I., Ostrand-Rosenberg, S., and Bronte, V. (2012). Coordinated regulation of myeloid cells by tumours. Nat. Rev. Immunol. *12*, 253–268.

Galluzzi, L., Senovilla, L., Zitvogel, L., and Kroemer, G. (2012). The secret ally: immunostimulation by anticancer drugs. Nat. Rev. Drug Discov. *11*, 215–233.

Gattinoni, L., Powell, D.J., Jr., Rosenberg, S.A., and Restifo, N.P. (2006). Adoptive immunotherapy for cancer: building on success. Nat. Rev. Immunol. *6*, 383–393.

Geissmann, F., Jung, S., and Littman, D.R. (2003). Blood monocytes consist of two principal subsets with distinct migratory properties. Immunity *19*, 71–82.

Ghiringhelli, F., Larmonier, N., Schmitt, E., Parcellier, A., Cathelin, D., Garrido, C., Chauffert, B., Solary, E., Bonnotte, B., and Martin, F. (2004). CD4+CD25+ regulatory T cells suppress tumor immunity but are sensitive to cyclophosphamide which allows immunotherapy of established tumors to be curative. Eur. J. Immunol. *34*, 336–344.

Ghiringhelli, F., Menard, C., Puig, P.E., Ladoire, S., Roux, S., Martin, F., Solary, E., Le Cesne, A., Zitvogel, L., and Chauffert, B. (2007). Metronomic cyclophosphamide regimen selectively depletes CD4+CD25+ regulatory T cells and restores T and NK effector functions in end stage cancer patients. Cancer Immunol. Immunother. *56*, 641–648.

Grivennikov, S.I., Greten, F.R., and Karin, M. (2010). Immunity, inflammation, and cancer. Cell *140*, 883–899.

Khanna, K.M., McNamara, J.T., and Lefrançois, L. (2007). In situ imaging of the endogenous CD8 T cell response to infection. Science *318*, 116–120.

Klebanoff, C.A., Khong, H.T., Antony, P.A., Palmer, D.C., and Restifo, N.P. (2005). Sinks, suppressors and antigen presenters: how lymphodepletion enhances T cell-mediated tumor immunotherapy. Trends Immunol. *26*, 111–117.

Kusmartsev, S., Nagaraj, S., and Gabrilovich, D.I. (2005). Tumor-associated CD8+ T cell tolerance induced by bone marrow-derived immature myeloid cells. J. Immunol. *175*, 4583–4592.

Lesokhin, A., Hohl, T.M., Kitano, S., Cortez, C., Hirschhorn-Cymerman, D., Avogadri, F., Rizzuto, G.A., Lazarus, J.J., Pamer, E.G., Houghton, A.N., et al. (2011). Monocytic CCR2+ myeloid derived suppressor cells promote immune escape by limiting activated CD8 T cell infiltration into the tumor microenvironment. Cancer Res. *72*, 876–86.

Lesokhin, A.M., Hohl, T.M., Kitano, S., Cortez, C., Hirschhorn-Cymerman, D., Avogadri, F., Rizzuto, G.A., Lazarus, J.J., Pamer, E.G., Houghton, A.N., et al. (2012). Monocytic CCR2(+) myeloid-derived suppressor cells promote immune escape by limiting activated CD8 T-cell infiltration into the tumor microenvironment. Cancer Res. *72*, 876–886.

Leuschner, F., Dutta, P., Gorbatov, R., Novobrantseva, T.I., Donahoe, J.S., Courties, G., Lee, K.M., Kim, J.I., Markmann, J.F., Marinelli, B., et al. (2011). Therapeutic siRNA silencing in inflammatory monocytes in mice. Nat. Biotechnol. *29*, 1005–1010.

Ma, Y., Kepp, O., Ghiringhelli, F., Apetoh, L., Aymeric, L., Locher, C., Tesniere, A., Martins, I., Ly, A., Haynes, N.M., et al. (2010). Chemotherapy and radiotherapy: cryptic anticancer vaccines. Semin. Immunol. *22*, 113–124.

Marigo, I., Bosio, E., Solito, S., Mesa, C., Fernandez, A., Dolcetti, L., Ugel, S., Sonda, N., Bicciato, S., Falisi, E., et al. (2010). Tumor-induced tolerance and immune suppression depend on the C/EBPbeta transcription factor. Immunity *32*, 790–802.

Molon, B., Ugel, S., Del Pozzo, F., Soldani, C., Zilio, S., Avella, D., De Palma, A., Mauri, P., Monegal, A., Rescigno, M., et al. (2011). Chemokine nitration prevents intratumoral infiltration of antigen-specific T cells. J. Exp. Med. *208*, 1949–1962.

Nagaraj, S., Gupta, K., Pisarev, V., Kinarsky, L., Sherman, S., Kang, L., Herber, D.L., Schneck, J., and Gabrilovich, D.I. (2007). Altered recognition of antigen is a mechanism of CD8+ T cell tolerance in cancer. Nat. Med. *13*, 828–835.

Ogawa, M., Matsuzaki, Y., Nishikawa, S., Hayashi, S., Kunisada, T., Sudo, T., Kina, T., Nakauchi, H., and Nishikawa, S. (1991). Expression and function of c-kit in hemopoietic progenitor cells. J. Exp. Med. *174*, 63–71.

Qian, B.Z., Li, J., Zhang, H., Kitamura, T., Zhang, J., Campion, L.R., Kaiser, E.A., Snyder, L.A., and Pollard, J.W. (2011). CCL2 recruits inflammatory monocytes to facilitate breast-tumour metastasis. Nature *475*, 222–225.

Restifo, N.P., Dudley, M.E., and Rosenberg, S.A. (2012). Adoptive immunotherapy for cancer: harnessing the T cell response. Nat. Rev. Immunol. *12*, 269–281.

Schreiber, R.D., Old, L.J., and Smyth, M.J. (2011). Cancer immunoediting: integrating immunity's roles in cancer suppression and promotion. Science *331*, 1565–1570.

Shi, C., and Pamer, E.G. (2011). Monocyte recruitment during infection and inflammation. Nat. Rev. Immunol. *11*, 762–774.

Shi, C., Jia, T., Mendez-Ferrer, S., Hohl, T.M., Serbina, N.V., Lipuma, L., Leiner, I., Li, M.O., Frenette, P.S., and Pamer, E.G. (2011). Bone marrow mesenchymal stem and progenitor cells induce monocyte emigration in response to circulating toll-like receptor ligands. Immunity *34*, 590–601.

Sica, A., and Bronte, V. (2007). Altered macrophage differentiation and immune dysfunction in tumor development. J. Clin. Invest. *117*, 1155–1166.

Solito, S., Falisi, E., Diaz-Montero, C.M., Doni, A., Pinton, L., Rosato, A., Francescato, S., Basso, G., Zanovello, P., Onicescu, G., et al. (2011). A human promyelocytic-like population is responsible for the immune suppression mediated by myeloid-derived suppressor cells. Blood *118*, 2254–2265.

Sonda, N., Chioda, M., Zilio, S., Simonato, F., and Bronte, V. (2011). Transcription factors in myeloid-derived suppressor cell recruitment and function. Curr. Opin. Immunol. *23*, 279–285.

Swirski, F.K., Nahrendorf, M., Etzrodt, M., Wildgruber, M., Cortez-Retamozo, V., Panizzi, P., Figueiredo, J.L., Kohler, R.H., Chudnovskiy, A., Waterman, P., et al. (2009). Identification of splenic reservoir monocytes and their deployment to inflammatory sites. Science *325*, 612–616.

Ugel, S., Scarselli, E., Iezzi, M., Mennuni, C., Pannellini, T., Calvaruso, F., Cipriani, B., De Palma, R., Ricci-Vitiani, L., Peranzoni, E., et al. (2010). Autoimmune B-cell lymphopenia after successful adoptive therapy with telomerase-specific T lymphocytes. Blood *115*, 1374–1384.

Vincent, J., Mignot, G., Chalmin, F., Ladoire, S., Bruchard, M., Chevriaux, A., Martin, F., Apetoh, L., Rébé, C., and Ghiringhelli, F. (2010). 5-Fluorouracil selectively kills tumor-associated myeloid-derived suppressor cells resulting in enhanced T cell-dependent antitumor immunity. Cancer Res. *70*, 3052–3061.

Walter, S., Weinschenk, T., Stenzl, A., Zdrojowy, R., Pluzanska, A., Szczylik, C., Staehler, M., Brugger, W., Dietrich, P.Y., Mendrzyk, R., et al. (2012). Multipeptide immune response to cancer vaccine IMA901 after single-dose cyclophosphamide associates with longer patient survival. Nat. Med. Published online July 29, 2012. http://dx.doi.org/10.1038/nm.2883.

Wrzesinski, C., and Restifo, N.P. (2005). Less is more: lymphodepletion followed by hematopoietic stem cell transplant augments adoptive T-cell-based anti-tumor immunotherapy. Curr. Opin. Immunol. *17*, 195–201.

Wrzesinski, C., Paulos, C.M., Kaiser, A., Muranski, P., Palmer, D.C., Gattinoni, L., Yu, Z., Rosenberg, S.A., and Restifo, N.P. (2010). Increased intensity lymphodepletion enhances tumor treatment efficacy of adoptively transferred tumor-specific T cells. J. Immunother. *33*, 1–7.

Zitvogel, L., Kepp, O., and Kroemer, G. (2011). Immune parameters affecting the efficacy of chemotherapeutic regimens. Nat. Rev. Clin. Oncol. *8*, 151–160.

Cell PRESS
Open ACCESS

EXTENDED EXPERIMENTAL PROCEDURES

Mice

Eight-week-old C57BL/6 (H-2^b) and BALB/c (H-2^d) mice were purchased from Charles River Laboratories Inc. OT-1 TCR-transgenic mice (C57Bl/6-Tg(TcraTcrb)1100Mjb/J), GFP reporter transgenic mice (C57BL/6-Tg(UBC-GFP)30Scha/J) and CD45.1^+ congenic mice (B6.SJL-$Ptrc^a Pepc^b$/BoyJ) were from Jackson Laboratories. pmel-1 TCR transgenic mice on C57BL/6 background were a gift from N. Restifo. B6.129S4-$Ccr2^{tm1Ifc}$/J and B6.129S4-$Ccl2^{tm1Rol}$/J mice were purchased from Jackson Laboratories, $Ccl2^{-/-}$ mice on BALB/c background were a gift from Dr. E.S Mocarski (Emory Vaccine Center, Atlanta, GA). H-2^b $Rag2^{-/-}\gamma_c^{-/-}$ mice were purchased from Taconics, H-2^d $Rag2^{-/-}\gamma_c^{-/-}$ mice were a gift from the Central Institute for Experimental Animals in Kawasaki, Japan. K^d-restricted $HA_{512\text{-}520}$ peptide-specific α/β TCR (CL4) mice were a gift from L. Sherman (The Scripps Research Institute, La Jolla, CA, USA). GFP-chimeric mice were generated by 900-rad γ-irradiation of GFP mice and reconstitution with $2x10^7$ C57BL/6 bone marrow cells. All mice were maintained under specific pathogen-free conditions in the animal facilities of the Istituto Oncologico Veneto, experiments were performed according to the national guidelines and approved by the local ethics committee.

Cell Lines

3-methylcholanthrene-induced MCA203 fibrosarcoma, TC-1 lung carcinoma, MBL-2 lymphoma, chicken ovalbumin (OVA)-transfected EL-4 (EG7) and EL-4 thymomas are all derived from C57BL/6 mice. CT26 colon carcinoma, 4T1 and 4T1-HA mammary carcinomas are derived from BALB/c mice. These cell lines were grown in DMEM (Invitrogen) supplemented with 2 mM L-glutamine, 10 mM HEPES, 20 μM β-mercaptoethanol, 150 U/ml streptomycin, 200 U/ml penicillin, and 10% heat-inactivated FBS (Invitrogen).

Cytokines, Reagents, and Synthetic Peptides

Mouse recombinant GM-CSF and mouse recombinant IL-6 were purchased from Peprotech Inc. K^b-restricted $OVA_{257\text{-}264}$ peptide (SIINFEKL), K^b-restricted $\beta\text{-gal}_{96\text{-}103}$ peptide (DAPIYTNV), D^b-restricted $hgp100_{25\text{–}33}$ peptide (KVPRNQDWL), K^b-restricted $mTERT_{198\text{-}205}$ peptide (VGRNFTNL) and K^d-restricted $HA_{512\text{-}520}$ (IYSTVASSL) peptide were synthesized by JPT (Berlin, Germany).

Chemotherapy Treatment

For in vivo experiments, mice received a single injection of 120 mg/kg gemcitabine (GEMZAR, Lilly), 10 mg/kg fludarabine (Fludara, Berlex), 20 mg/kg cyclophosphamide (Cytoxan, Bristol-MyersSquibb), 40 mg/kg 5-fluorouracil (Valeant Pharmaceuticals), 50 mg/kg cisplatin (Cisplatine-Mepha, Mepha Pharma), 10 mg/kg docetaxel (Taxotere, Sanofi Aventis), 10 mg/kg etoposide (Vp-16, Novopharm), 4 mg/kg bortezomib (Velcade, Millenium Pharmaceuticals), 10 mg/kg vinblastine (Velbe, Crinos), 5 mg/kg doxorubicin (Rubex, Pfizer), 60 mg/kg sunitinib (Sutent, Pfizer), and 40 mg/kg sorafenib (Nexavar, Bayer). All drugs were administrated by i.p. injection, except for doxorubicin and vinblastine, which were i.v. injected, while sunitinib and sorafenib, which were orally administered by oral gavage.

Lymphocyte Cultures

mTERT- and β-gal-specific CTLs were maintained in culture with γ-irradiated syngeneic splenocytes pulsed with either 0.1 μM of $TERT_{198\text{-}205}$ or 1 μM of $\beta\text{-gal}_{96\text{-}103}$ peptides. Cultures were grown for 7 days in complete medium containing 20 IU/ml of recombinant human IL-2 (Novartis).

Myeloid Cell Transfer

$Rag2^{-/-}\gamma_c^{-/-}$ mice were subcutaneously challenged with $1x10^6$ MCA203 cells. When tumor volume was about 200 mm^3, mice were treated with 40 mg/kg 5-FU by a single i.p. injection. After 2 days, mice were adoptively transferred, via i.v. injection, with $5x10^6$ immunomagnetically sorted $CD11b^+Gr\text{-}1^{int}$ or $CD11b^+Gr\text{-}1^{hi}$ cells. The day after mice received $5x10^6$ antigen-specific CTLs. Blind measurements of tumor mass were carried out using digital calipers. Mice were euthanized when tumor volume reached 1,000 mm^3.

In Vivo Proliferation Assay

For BrdU analysis, mice were i.p. injected with BrdU (7.2 mg/kg, Sigma) either 2 hr or 48 hr before analysis. At sacrifice, bone marrow cells and splenocytes were isolated and labeled with anti-CD11b and anti-Gr-1 antibodies, followed by BrdU detection performed with the appropriate BD Biosciences kit. When proliferation was measured ex vivo, Ki-67 staining was performed according to BD Biosciences protocol.

Cytological Preparation

$1x10^5$ sorted cell subsets were spun over slides with a Shandon Cytospin for 4 min at 800 rpm, with 1 min at 800 rpm preconditioning. Cells were fixed in -20°C cold methanol for 20 min. Slides were stained for 2 min in 1:1 May–Grünwald/phosphate buffer pH 6.8 and for 20 min in 6% Giemsa in phosphate buffer pH6.8.

In Vitro Myeloid Cell Differentiation

FACS-sorted myeloid cell subsets were plated in 6-well plates ($2x10^6$ cells/well) for 48 hr with GM-CSF (40 ng/ml) and IL-6 (40 ng/ml) and harvested by washing with PBS 2 mM EDTA.

In Vivo Myeloid Differentiation

Donor CD45.1 C57BL/6 mice were injected with $1x10^6$ EL4 cells (s.c.) in the flank. After 2 weeks myeloid cell subsets were FACS-sorted from the spleen according to CD11b and Gr-1 expression and $1x10^6$ sorted cells/mouse were i.v. injected into CD45.2 C57BL/6 mice, that had received EL4 cells 1 week earlier. CD45.1 myeloid cell differentiation was monitored in recipient CD45.2 mice 1 week after the adoptive transfer.

CFU Assay

FACS-sorted splenocytes were cultured on MethoCult GF M3434 medium (STEMCELL Technologies) and colonies were evaluated from day 7 to day 14. $1.5x10^4$ cells/well were plated in 24-well plates.

Flow Cytometry

Single-cell suspensions were labeled with fluorochrome-conjugated mAb anti-mouse CD11b (M1/70), Gr-1 (RB6-8C5), Ly6C (HK1.4), Ly6G (1A8), F4/80 (Cl:A3-1), IL-4Rα (mIL4R-M1), CD115 (AFS98), CD68 (ED1), CD62L (MEL-14), CD117 (2B8), Sca-1 (D7), MHC II (2G9), CD3 (145-2C11), CD8 (53-6.7), CD44 (IM7), CD127 (SB/199), CD25 (PC61), CD45R/B220 (RA3-6B2), $_{\alpha/\beta}$TCR (H57-597), CD45 (30-F11), CD45.1 (A20), CD45.2 (104), IFN-γ (XMG1.2), CCR2 (475301), MHC I-OVA (eBio25-D1.16), Ki-67 (35) antibodies and matched isotypes, purchased from either BD Biosciences, eBiosciences, Serotec, R&D or Biolegend. All samples were acquired with a FACSCalibur™ (BD) and analyzed with FlowJo software (Treestar Inc.).

Immunofluorescence

Tissues were fixed with PBS PFA 4% for 3 hr at 4°C; dehydration was performed with 20% and 30% sucrose, for one or three days respectively. Tissues were frozen in Optimal Cutting Temperature (Killik, Bio-Optica). Transverse cryosections (8–10 μm) were post-fixed 5′ RT with PBS PFA 4%. Blocking was performed for 30' at RT with PBS 10% FBS 0.1% Tween. Primary antibody rat anti-mCD8 (YTS169.4) was applied 2 hr at 37°C. Secondary donkey anti-rat RRX was incubated 1 hr at 37°C. Primary rat anti-mouse Ly6C-FITC (AL-21) and rat anti-mouse CD19-Alexa647 (eBio1D3) antibodies were incubated ON at 4°C. DNA counterstaining was performed with either DAPI (1μg/ml, Sigma) or TOPRO-3 (1μg/ml, Invitrogen), 10' at RT. Samples were mounted with ProLong Antifade (Invitrogen). Following the same protocol, other antibodies were also used: anti-CD31 Alexa647 (390), anti-Ly6G FITC (1A8), anti-rabbit MCP-1 pAb (Ab7202), Donkey anti-rabbit Dylight649. Images were acquired with a Leica LS5 confocal microscope equipped with UV, Ar and He lasers. Interfollicular area was calculated as the difference between the total area of splenic sections and the follicular area (identified by CD19). Colocalization analysis between $Ly6C^+$ monocytes and $Ly6C^+CD8^+$ or $Ly6C^-CD8^+$ lymphocytes was performed as described in Figure S5. These analyses were performed with ImageJ software.

In Vitro CTL Stimulation

CTLs were stimulated in vitro with two different procedures: mixed lymphocyte reaction (MLR) and mixed leukocyte peptide culture (MLPC). In MLRs, $6x10^5$ splenocytes from either healthy or tumor-bearing C57BL/6 mice were incubated with $6x10^5$ γ-irradiated BALB/c splenocytes. MLPCs were set up with C57BL/6 splenocytes cultured for 5 days together with either 1% OVA-specific $CD8^+$ T lymphocytes, derived from the spleen of OT-1 transgenic mice, or 1% gp100-specific $CD8^+$ T lymphocytes, derived from the spleen of *pmel*-1 transgenic mice. Splenocytes were pulsed with either 1 μg/ml $hgp100_{25–33}$ or $OVA_{257-264}$ peptide. $CD11b^+$ cells, syngeneic to responder splenocytes, were added to the cultures in serial dilution ranging from 48 to 1.5% of total culture cell number.

Lymphocyte Proliferation by CFSE Dilution

MLPCs were set up with C57BL/6 splenocytes pulsed with 1 μg/ml $gp100_{25–33}$ or $OVA_{257-264}$ peptide and cultured together with 1% CFSE-labeled (1 μM CFSE), gp100- or OVA-specific $CD8^+$ T lymphocytes, derived from the spleens of *pmel-1* or OT-1 transgenic mice. CFSE dilution in $CD8^+$ T cells was assessed 3 days later by flow cytometry.

Enzyme-Linked Immunosorbent Assay

E.L.I.S.A. for murine CCL2 was performed with an eBioscience kit, following manufacturer's instructions.

Lymphocyte Transfer

$Rag2^{-/-}\gamma_c^{-/-}$ mice were s.c. implanted with MCA203 sarcoma cells and treated with a single dose of 5-FU after 3 hr. After 2 days, $1x10^6$ of $Ly6C^+CD8^+$, $Ly6C^-CD8^+$ or $CD4^+$ T cells were injected i.v. in the same mice. $Rag2^{-/-}\gamma_c^{-/-}$ mice were sacrificed at different times after chemotherapeutic treatment.

Monitoring of T Cell Responses in Cancer Patients

In both clinical trials, immunomonitoring for all individual HLA-A*02 associated peptides of the vaccines were performed, based on PBMCs isolated from two time points before the first vaccination and multiple time points after vaccination, according to a standardized, predefined blood collection schedule. PBMCs were isolated from patients within 8 hr of venipuncture using fully standardized procedures, cryopreserved and shipped for central laboratory analysis. T cell responses to individual A*02-binding peptides were then analyzed after antigen stimulation and 12-day in vitro culture by performing HLA-multimer staining and IFNγ ELISPOT (RCC phase II study) or HLA-multimer staining and ICS for IFNγ, TNFα, MIP1β, IL10 and CD107α (CRC phase I/II study IMA910-101). Presence or absence of vaccine-induced responses to individual HLA-A*02 binding peptides were detected by comparing post-vaccination to prevaccination samples, according to objective criteria predefined in the respective statistical analysis plans. 61/64 PP RCC patients and 81/82 PP CRC patients were evaluable for T cell response analysis of all HLA-A*02 associated peptides.

Analysis of Myeloid Subsets among PBMCs of Cancer Patients

Frequencies of myeloid cells were assessed by ex vivo multicolor flow cytometric analysis of PBMCs obtained prior to treatment. PBMC samples were thawed in the presence of 0.5 U/ml Benzonase (Merck). Cells were first stained with the LIVE/DEAD fixable Aqua dead cell stain kit and then blocked with hIgG (AbD Serotec) to reduce subsequent Fc-mediated binding. Cells were then surface stained with anti-CD45 (Life technologies) and anti-CD15, CD11b, CD124, CD14, CD33, Lin (CD3, CD14, CD19, CD56) and CD45 (BD Biosciences). After erythrocyte lysis and fixation with FACS lysing solution (BD Biosciences), measurement was performed on a LSR II SORP instrument (BD Biosciences). All samples were analyzed in one experiment. Primary data analysis was performed with FlowJo (TreeStar). Identical gates were used for analysis of all samples of one study. Samples were set evaluable if at least 75.000 viable $CD45^+$ cells were counted. A total of 61/68 RCC patients and 89/92 CRC patients were evaluable for MDSC analysis.

CCL2 Measurement in Cancer Patients

Sera of renal cancer carcinoma (RCC) and colon cancer carcinoma (CRC) patients were collected prior to vaccination. Samples were taken using a serum/gel-Vacutainer (Becton Dickinson, 5 mL), inverted and incubated for a minimum of 30 min. Tubes were centrifuged for 15 min at at least 1,200x*g*, and serum was transferred into a NUNC cryotube, stored immediately at -20°C until measurement. CCL2 in RCC patient sera was measured by Rules Based Medicine (RBM), Austin, TX, using Luminex technology. CCL2 in CRC patient sera was measured by Aushon, Billerica, MA using a custom 37-plex spotted chemiluminescent antibody array.

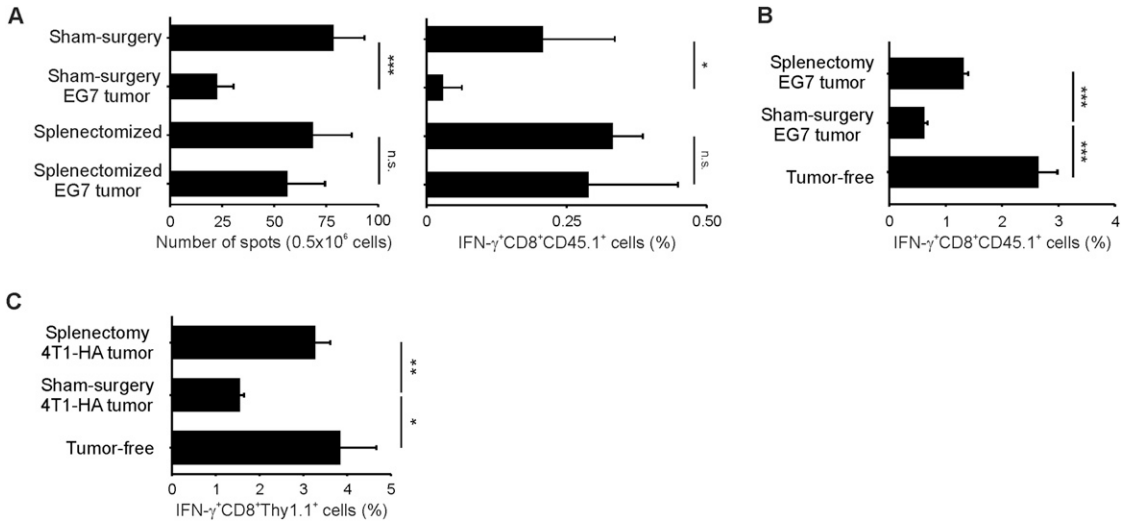

Figure S1. Splenectomy Affects Memory CD8$^+$ T Cell Tolerization, Related to Figure 1

(A) Experiment performed as described in Figure 1B except that Ag-primed instead of naïve CD8$^+$ T cells were adoptively transferred. Fourteen days after splenectomy or sham surgery, C57BL/6 mice were either s.c. injected or not with 1 × 10^6 EG7 tumor cells. After 7 days, mice were treated with 5 × 10^6 Ag-primed OVA-specific CD8$^+$ T cells. At day 14, draining lymph nodes were removed and tested for IFN-γ production by ELISpot assay (left panel) and intracellular staining (right panel). Data are presented as mean ± SD (n = 3 mice/group for each experiment) of two independent experiments. Statistical analysis was performed with Student's t test.

(B) Experiment performed as described in (A), except that mice were inoculated with 2 × 10^7 OT-1 naïve splenocytes and vaccinated with OVA peptide-pulsed DCs 2 days after ACT. Data are presented as mean ± SD (n = 3 mice/group for each experiment) of three independent experiments. Statistical analysis was performed with Student's t test.

(C) Splenectomy or sham surgery was performed on BALB/c background mice. Ten days after surgery, mice were s.c. injected with 1 × 10^6 4T1-HA tumor cells. After 20 days, mice were transferred with 2 × 10^7 splenocytes derived from CL4 mice. Two days after ACT, mice were vaccinated with HA peptide-pulsed DCs. At day 26, lymph nodes were assessed for IFN-γ production by means of intracellular staining. Data are presented as mean ± SD (n = 7 mice/group) of one representative experiment. Statistical analysis was performed with Student's t test.

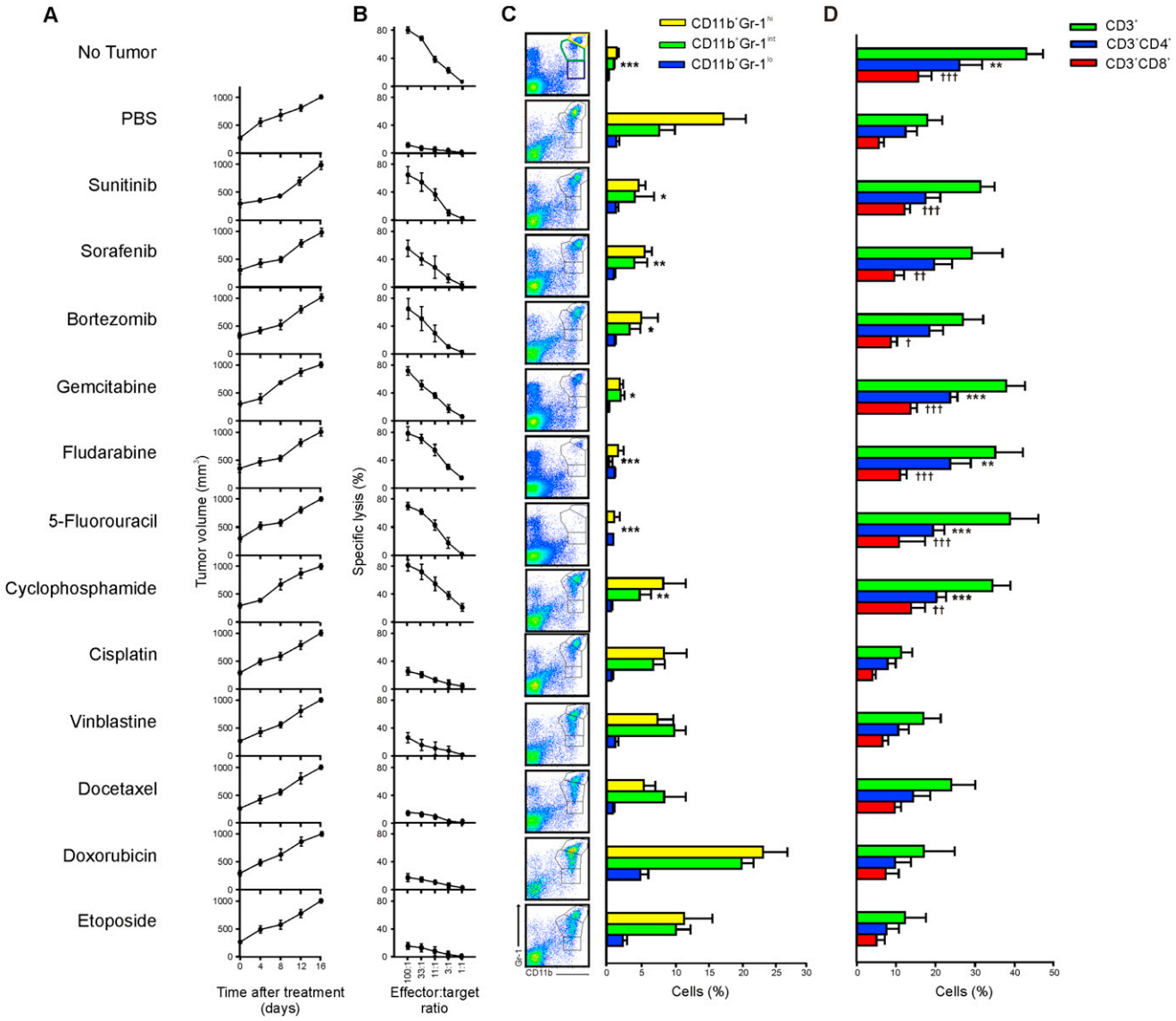

Figure S2. Chemotherapy Restores Immune Responsiveness in Tumor-Bearing Mice, Related to Figure 2

(A) Tumor growth curves of mice treated with different chemotherapeutic drugs. Mice were s.c. injected with 1×10^6 MCA203 sarcoma cells in the right flank. Two weeks after tumor injection, when tumor volume was ~400 mm^3, mice were treated with the indicated drugs. Data are representative of two independent experiments.

(B) Sixteen days after chemotherapy, mice were sacrificed to test their immune responsiveness. Splenocytes were incubated with γ-irradiated allogeneic splenocytes in a standard allogeneic MLC culture. After 5 days, alloreactive T lymphocytes were tested in a ^{51}Cr release assay. Data are representative of two independent experiments.

(C) Splenocytes from drug-treated mice were analyzed for CD11b and Gr-1 expression by flow cytometry. Gr-1/CD11b dot plots illustrate the gate setting (left panels). The percentages of $CD11b^+Gr\text{-}1^{hi}$, $CD11b^+Gr\text{-}1^{int}$ and $CD11b^+Gr\text{-}1^{lo}$cells are presented as mean ± SD (n = 3 mice/group for each experiment) of two independent experiments. Wilcoxon's rank sum test was performed to compare PBS- versus drug-treated tumor-bearing mice.

(D) Splenocytes from drug-treated mice were analyzed for CD3, CD4, and CD8 expression by flow cytometry. The percentage of $CD3^+$, $CD3^+CD4^+$, and $CD3^+CD8^+$ cells is represented as mean ± SD (n = 3 mice/group for each experiment) of two independent experiments. Wilcoxon's rank sum test was performed to compare PBS- versus drug-treated tumor-bearing mice, for either $CD3^+CD4^+$ (*) or $CD3^+CD8^+$ (†) cells. * or † $p < 0.05$, ** or †† $p < 0.01$, *** or ††† $p < 0.001$.

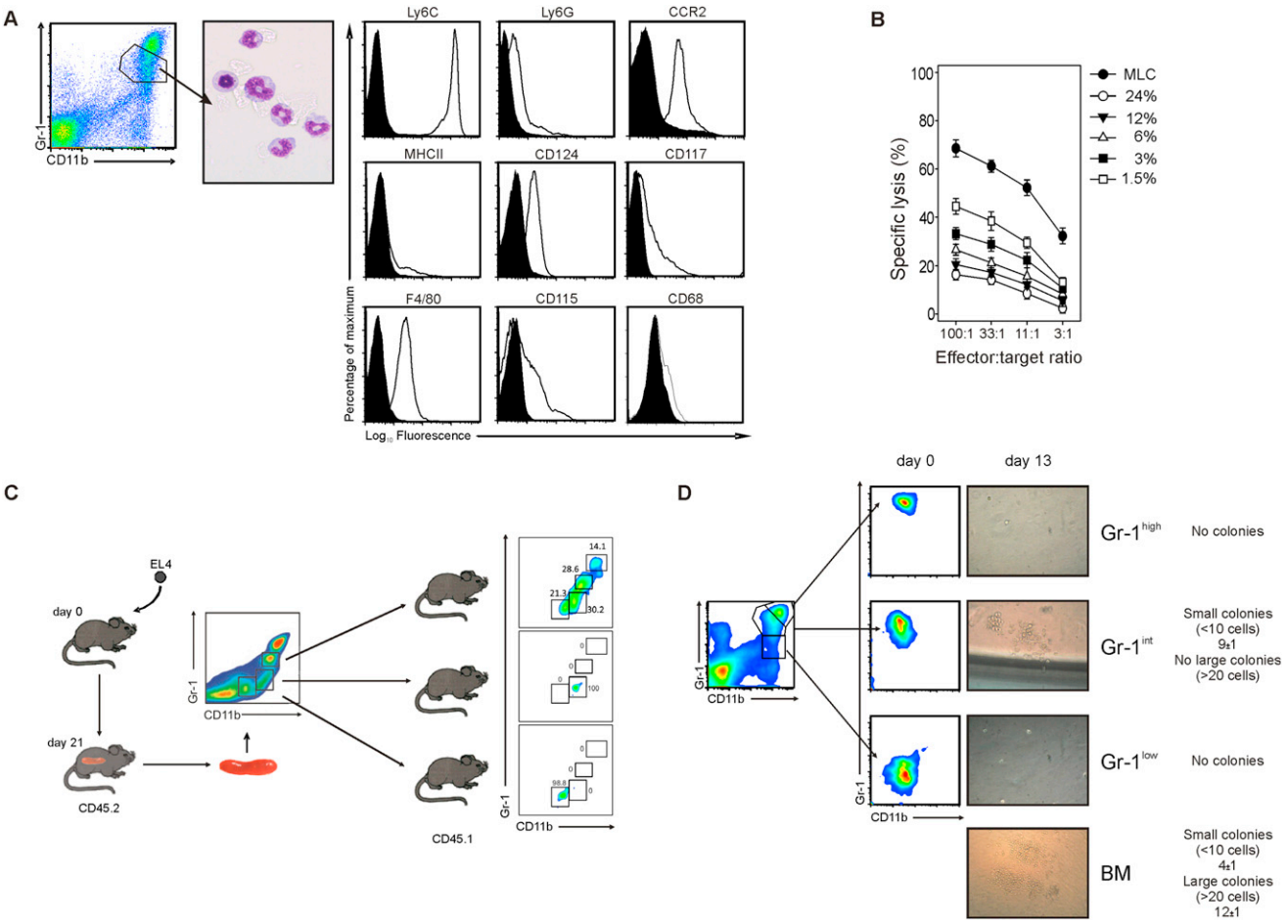

Figure S3. CD11b^{+}Gr-1^{int} Cells Resemble Multipotent Inflammatory Monocytes, Related to Figure 3

(A) CD11b^{+}Gr-1^{int} cells were FACS-sorted as indicated and analyzed for morphology by May-Grünwald-Giemsa staining (left panel) and phenotype by flow cytometry (right panel).

(B) The suppressive activity of FACS-sorted CD11b^{+}Gr-1^{int} cells was evaluated by adding different percentages of sorted cells to an allogeneic MLC and testing for cultured T cell cytotoxicity with a ^{51}Cr-release assay.

(C) Adult CD45.2 C57BL/6 mice were injected with 1 × 10^{6} syngeneic EL4 mouse thymoma cells. CD11b^{+}Gr-1^{int}, CD11b^{+}Gr-1^{lo}, and CD11b^{+}Gr-1^{-} cells were sorted from the spleens of tumor-bearing mice 3 weeks after implantation. Sorted cells were adoptively transferred to adult tumor-free CD45.1 C57BL/6 mice. The phenotype of CD45.2 cells was analyzed 5 days after adoptive transfer by flow cytometry. Dot-plots show the percentage of CD11b^{+}Gr-1^{+} splenic cells. Results represent the mean (n = 4 mice) of a representative experiment.

(D) CD11b^{+}Gr-1^{+} cells were FACS-sorted as indicated and 1.5 × 10^{4} cells were plated in MethoCult methylcellulose-based media. Unfractionated bone marrow cells were plated as a control. CFUs were counted from day 7 to day 14. Data are presented as mean ± SD at day 14 of two independent experiments (n = 3 mice for each experiment).

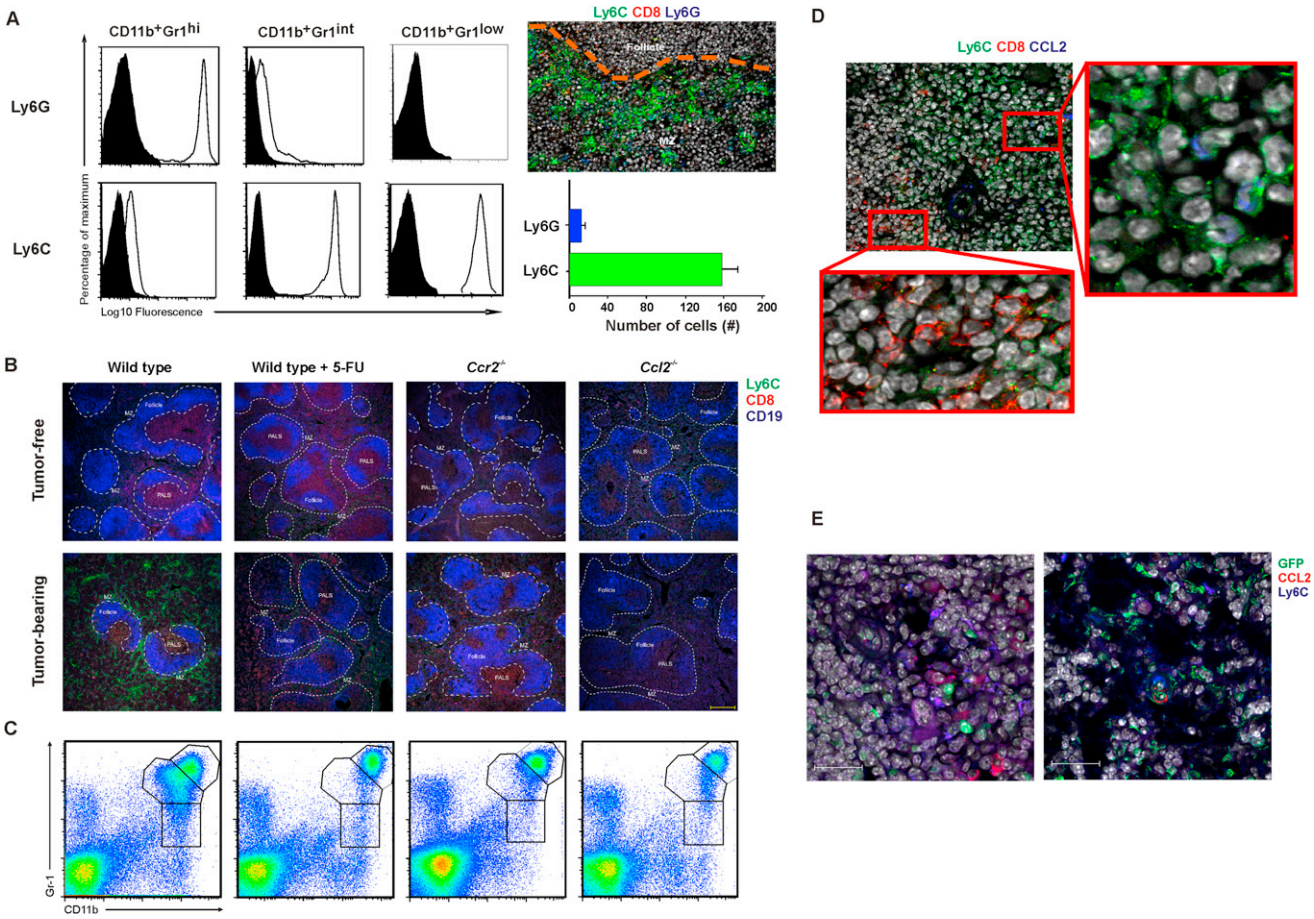

Figure S4. CCL2 Production in the Spleen, Related to Figure 4

(A) CD11b$^+$Gr-1^{hi}, CD11b$^+$Gr-1^{int} and CD11b$^+$Gr-1^{low} cells were isolated from splenocytes of EG7 tumor-bearing mice by cytofluorimetric sorting and then stained with anti-Ly6C and anti-Ly6G mAbs. CD11b$^+$Gr-1^{hi} cells are prevalently Ly-6G-positive cells, whereas CD11b$^+$Gr-1^{int} cells express high levels of Ly-6C. Ly-6C is also expressed by Gr-1^{low} cells, which represent a minor fraction of the total CD11b$^+$Gr-1$^+$ cells. Taking advantage of this observation, we decided to use Ly6C as marker to track CD11b$^+$Gr-1^{int} cells, and Ly6G as a marker to define CD11b$^+$Gr-1^{hi} cells by confocal microscopy (upper right). A predominant accumulation of Ly6C positive cells was observed in the MZ of the spleen of tumor-bearing mice (upper right). Ly6G$^+$ Ly6C$^-$ constituted only about 8% of the total myeloid cells surrounding CD8$^+$ T cells in the MZ (lower right).

(B) Spleen architecture was assessed by immunofluorescence on thin cryosections. Samples were labeled for Ly6C (green), CD8 (red), and CD19 (blue). Spleens were collected from either tumor-free mice or mice bearing an ~600 mm^3 subcutaneous MCA203 fibrosarcoma, either treated or not for 25 days with 5-FU. B cells are located in the lymphoid follicles, T cells are located around the central arteries to form aggregates called the periarteriolar lymphoid sheath (PALS). The white pulp is bordered innermost by the MZ and outermost by the red pulp. Ly6C$^+$ cells localize to the MZ. In tumor-bearing mice, MZ was hyperplastic to the detriment of the PALS, and this aspect was reversed by 5-FU treatment and *Ccr2*$^{-/-}$ and *Ccl2*$^{-/-}$ mice. Follicles are indicated by dotted lines. The interfollicular area was calculated as the difference between the total area of the section and the sum of follicular areas (CD19-positive areas). Scale bars are 250 μm.

(C) Representative dot-plots of myeloid cell distribution in splenocytes stained for anti-CD11b and anti-Gr-1 antibodies. This gating setting was used to analyze splenocyte phenotype in Figure 4B.

(D) A representative image of the spleen of MCA203 tumor-bearing mice stained with anti-Ly6C, anti-CCL2, and anti-CD8 specific mAbs. The cytokine production was never detected in CD8$^+$ and CD8$^+$Ly6C$^+$ cells (lower panel magnification), whereas CCL2 was detected in Ly6C$^+$ cells (CCL2 signal is present inside the cytoplasmatic membrane; right panel magnification). This is a demonstration that only myeloid (and not lymphoid) Ly6C$^+$ cells contribute to CCL2 secretion in the spleen.

(E) Thin spleen cryosections from C57BL/6 → UBC-GFP bone marrow chimeras bearing MCA203 tumors. Chimeras were generated by sublethal irradiation (900 rad) of UBC-GFP recipient mice, subsequently transferred with 2 × 10^7 bone marrow cells from C57BL/6 donors. GFP-positive cells (green) represent cells of recipient origin, and GFP-negative cells are bone-marrow-derived donor cells. Scale bars are 50 μm.

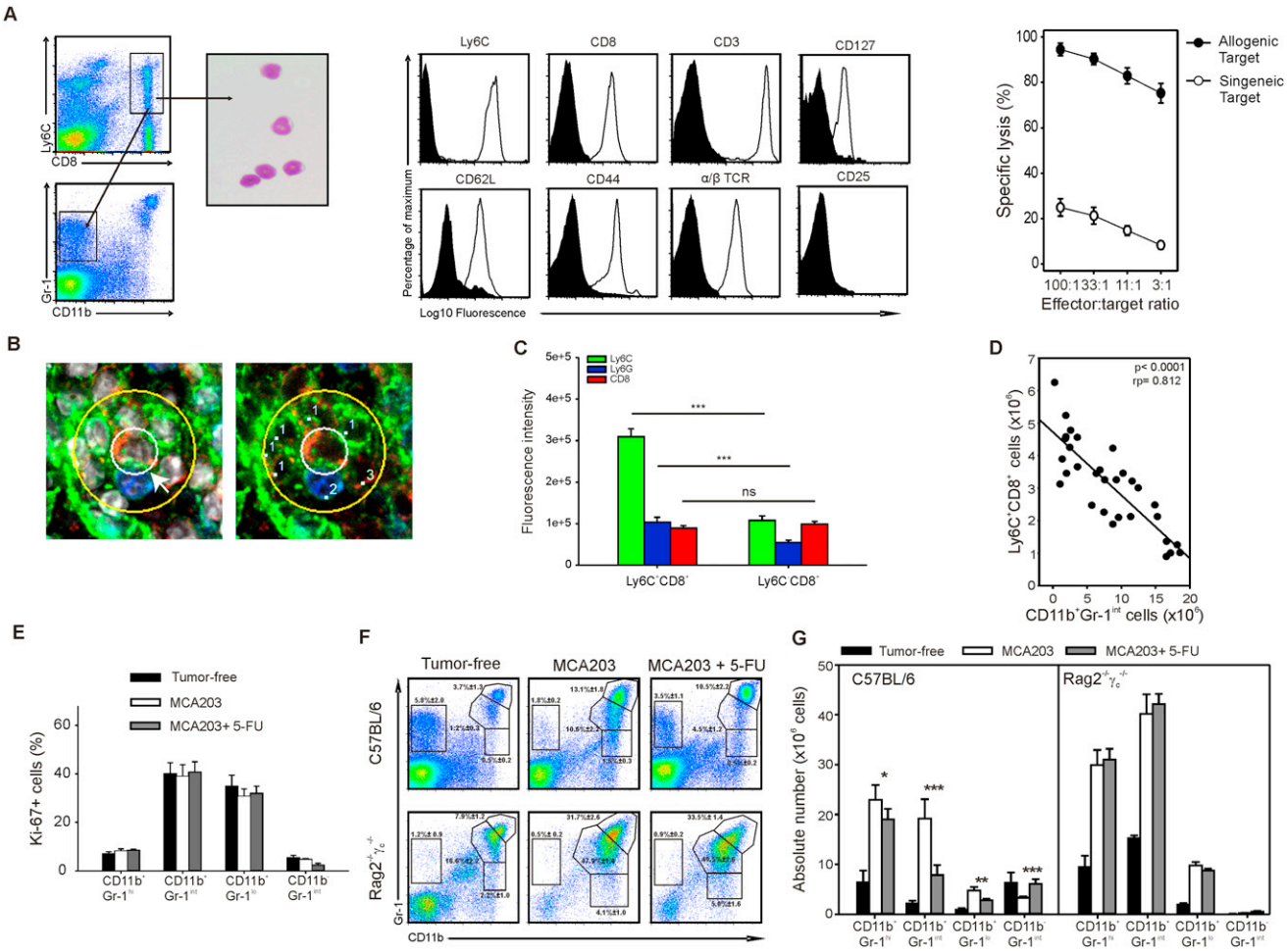

Figure S5. Ly6C$^+$ Myeloid Cells Colocalize and Reciprocally Interfere with Ly6C$^+$CD8$^+$ T Cells with a Central Memory Phenotype, Related to Figure 5

(A) Representative dot-plots of the gating strategy, showing CD8 versus Ly6C and CD11b versus Gr-1 staining of splenocytes from tumor-free mice. FACS-sorted splenic Ly6C$^+$CD8$^+$ cells were assessed for cell morphology by May-Grünwald-Giemsa staining (left panel), full surface molecule phenotype (central panel), and function (right panel). For functional assessment, Ly6C$^+$CD8$^+$ were cocultured in the presence of γ-irradiated allogenic splenocytes for 5 days and then tested in a ^{51}Cr release assay against allogenic and syngeneic target cells.

(B) Strategy used to quantify the number of cells and fluorescence intensity of cells surrounding either Ly6C$^+$CD8$^+$ or Ly6C$^-$CD8$^+$ T cells. The cell of interest was framed in the small area (white), and a concentrically larger area approximately corresponding to one cell diameter (yellow) was drawn. The total fluorescence of that area was automatically calculated using ImageJ, while the number of cells was manually numbered and subdivided into three groups: (i) Ly6C$^+$Ly6G$^-$CD8$^-$ (Ly6C$^+$), (ii) Ly6C$^{+/-}$Ly6G$^+$CD8$^-$ (Ly6G$^+$), and (iii) Ly6C$^-$Ly6G$^-$CD8$^+$ (CD8$^+$). CD8$^+$ T cells were classified as either Ly6C$^+$ or Ly6C$^-$ by considering the number of pixels that were positive for both fluorochromes. This analysis was performed using the Intensity Correlation Analysis plugin of ImageJ v1.46i.

(C) Quantification of the fluorescence intensity on the ring region (yellow area-white area) surrounding either Ly6C$^+$CD8$^+$ or Ly6C$^-$CD8$^+$ T cells. Data are presented as mean ± SE (n = 70 area for each group). Statistical analysis was performed with Student's t test.

(D) Correlation between absolute numbers of CD11b$^+$Gr-1^{int} and CD11b$^-$Gr-1^{int} cells during tumor progression in immunocompetent MCA203 tumor-bearing mice.

(E) Proliferative potential of different splenocyte subsets of healthy, untreated tumor-bearing mice and 5-FU-treated, tumor-bearing mice. Ex vivo proliferation was measured ex vivo by means of Ki-67 intracellular staining. Data are represented as mean ± SE (n = 3 mice/group) of one representative experiment out of two independently performed experiments.

(F) C57BL/6 and *Rag2*$^{-/-}\gamma_c^{-/-}$ mice were s.c. implanted with 1 × 10^6 MCA203 cells and treated with a single dose of 5-FU after 3 hr. Mice were sacrificed 30 days later and CD11b$^+$Gr-1$^+$ splenocyte distribution was analyzed.

(G) Absolute numbers of different cell subsets are reported as mean ± SD (n = 3 mice/group). Wilcoxon's rank sum test was performed to compare MCA203 and MCA203+5-FU groups.

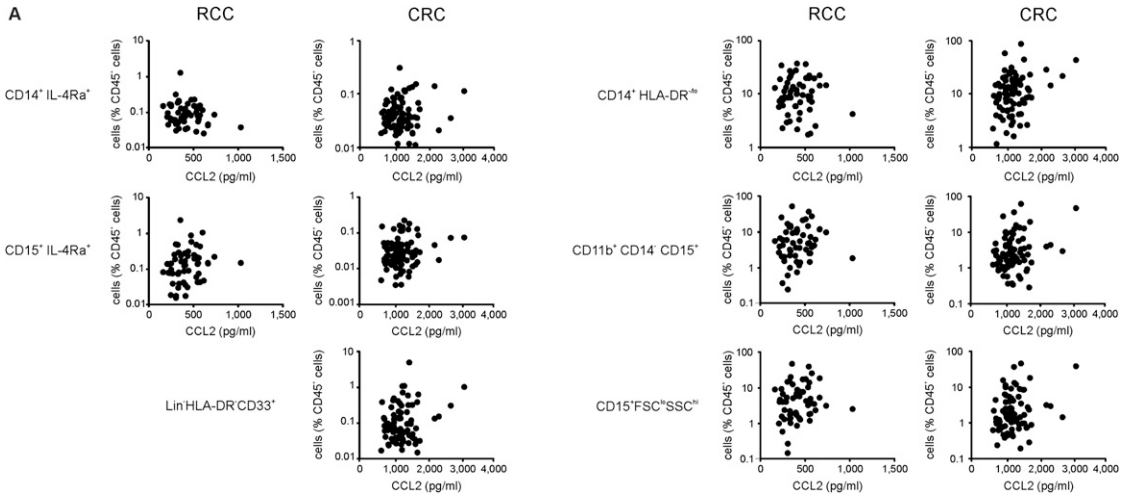

Figure S6. Correlation Analysis between Myeloid Cell Subset Frequencies and CCL2 Levels in the Serum of Cancer Patients, Related to Figure 6

Correlation analysis of serum CCL2 concentration and different subsets of peripheral blood myeloid cell in individual cancer patients determined prior to immunotherapy; n = 58 (RCC) and n = 85 (CRC) patients were evaluable for analysis; · represents individual patients.